Damage Evaluation of a Three-story Composite Steel Frame subjected to External Explosion

*Tarek Sharaf[1], Sara Ismail[2 *], Mohamed Elghandour[3], Ahmed Turk[4]*

[1] *Civil Engineering Department, Faculty of Engineering, Port Said University, Port said, Egypt, email: tarek.sharaf@eng.psu.edu.eg,*

[2] *Civil Engineering Department, Faculty of Engineering, Port Said University, Port said, Egypt, email: sara.ismail@eng.psu.edu.eg,*

[3] *Civil Engineering Department, Faculty of Engineering, Port Said University, Port said, Egypt, email: dr.elghandor@gmail.com,*

[4] *Civil Engineering Department, Faculty of Engineering, Port Said University, Port said, Egypt, email: ahmed.adel@eng.psu.edu.eg*

*Corresponding author, DOI: 10.21608/PSERJ.2023.215946.1247

ABSTRACT

This paper investigated the blast performance of a three-storey composite steel building subjected to external explosion by a package bomb. Analysis was based on load combinations and damage criteria in accordance with three general design approaches relevant for civil design applications in predicting blast loads and structural system responses. The main objective is to provide a rapid blast evaluation and simplify the model when blast wave first impacts the structure. For first dynamic stage, direct simulation method was chosen for modelling blast loads on members exposed to explosion using the Friedlander blast load equation, and an empirical A.T.-BLAST method estimated its parameters to deduce the simplified blast-wave overpressure profile. For second static stage, the original Alternate Load Path method was used to check the probable stability of columns' damage due to heat after blast on adjacent elements using the standard temperature-time curve due to local fire. Results showed that structural elements were deformed away from their elastic limit and yield points, resulting in plastic behavior with considerable post-yielding deformations so ductility ratio, plastic hinge rotation, internal forces limits, Demand-Capacity-Ratio (DCR shear/moment) and material damage model are the judged adequacy in blast design and structural members' evaluation considering blast load as the initial cause of failure. After explosion, re-loading process resulted in structure' stability (non-collapse) due to ductility and introduced vierendeel effect to be reused again. Some guidelines have un-provided data on damage evaluation limit criteria while others overestimate the realistic damage conditions.

Keywords: Composite steel frame, Blast prediction, Direct simulation method, SCI, UFC and GSA guidelines, Damage criteria, ALP method.

1. INTRODUCTION

Extra-ordinary hazards as explosions, vehicle collision, and catastrophic fire or natural disasters such as earthquakes could result in progressive collapse of structures. An explosion is described as a rapid and violent release of energy in a short period of time using free gases at high pressures.

Hence, explosions can be classified into four types based on the source and the type of energy release, namely physical, nuclear, electrical or chemical, based on the nature of explosion. Another classification is based on confinement into internal explosion (confined) that occurs within the structure and external explosion (unconfined) that occurs in free air [1-3].

According to external explosion, hemispherical surface blast can be defined as detonations that are near to the ground or indefinite stiff objects, resulting in wave parameter amplification. Hence, surface burst occurs if an explosive charge is near or on the ground surface.

High explosives generate gases at pressures of up to 30,000 MPa and temperatures ranging from 3000° C to 4000° C [3, 4].

As the quantities of explosive charges are various in both composition and detonation pressure, there is a need for conversion factor or a reference explosive to compare the blast wave parameters produced by various explosive materials. This factor is called "TNT equivalence factor" that is provided in UFC 3-340-02 (Unified Facilities Criteria) [5] for several explosive materials and it is equal to 1.00 for TNT.

1.1 Blast Prediction and Simulation Methods

A pressure time history profile best represents the propagation of a free-air or surface burst. The primary goal of explosive scaling is to assess the effect of overpressure on different TNT explosives at various distances, so that blast loadings may be calculated using empirical formulas. These relationships are based on the principle of the scaling law [6]. The Hopkinson-Cranz blast scaling law is the most widely used blast scaling law, in which two explosive charges of comparable geometry different weights are detonated at equivalent scaled distances Z, producing similar blast waves. The scaled distance or the proximity factor (Z) in $m/kg^{1/3}$ is defined as:

$$Z = \frac{R}{W^{\frac{1}{3}}} \tag{1}$$

Where, Z is the scaled distance in $m/kg^{1/3}$, R is the range from center of the spherical charge to target or stand-off distance in meter and W is the mass of the spherical TNT charge in kg. This law is mentioned in current design regulations, such as SCI publication 244 [7]. The other important factor is the incidence angle, αa that is impacts blast wave reflection, amplifying blast pressure intensity [4]. (In this study, the reflection phenomenon was ignored).

The other blast parameters prediction using theoretical and empirical methods are available in literature by previous studies [2, 4, 5]. However, these parameters are used for calculation purposes to deduce the typical blast overpressure-time history that is called "the Friedlander waveform". This waveform had undergone many modifications and most common form nowadays is the modified Friedlander's equation that is frequently defined as an exponential decay function to display a blast's pressure profile, and it is expressed as [8]:

$$P(t) = P_o + P_{so}\, e^{-\frac{bt}{t_d}}\left(1 - \frac{t}{t_d}\right) \tag{2}$$

Where, P_o is the atmospheric pressure which is normally 100 kN/m^2, P_{so} is the peak incident overpressure, td is the positive phase duration which is

the time duration of the pressure that remain above the ambient pressure, t is measured from arrival time of blast wave t_a and b is the wave decay coefficient which is a dimensionless value and also if its value is less than one, the negative phase is important but becomes less significant if its value is greater than one.

For any analysis of structure, calculation of the pressure load acting on structure subjected to explosion is obtained by the pressure-time curve that is preferred to describe the blast wave as a triangle pulse in order to simplify the curving portion of the actual blast wave is characterized by maximum peak pressure incident, P_{so}. Different blast wave profiles are shown in Figure 1 by [1].
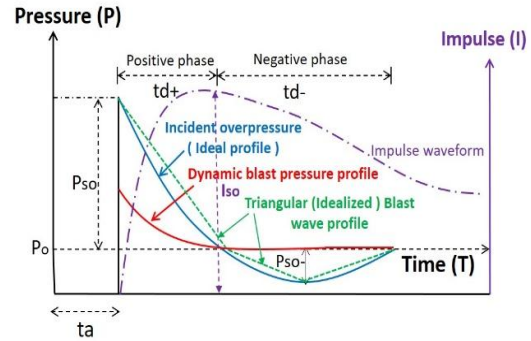
Figure 1: Blast wave profiles by [1]: ideal profile (Friedlander waveform), dynamic profile, triangular profile and impulse waveform

Generally, computational methods are effective design tools due to lower cost with improved accuracy. In addition, the common methods for numerically simulating blast wave propagation are based on the finite element method (FEM) that is preferred in this study for modelling blast phenomena because of its ability to model overall structural behavior under blast loads, interaction of structural members, and effects of geometric and material nonlinearity. It also captures the plastic hinge formation, defines deflection, ductility, and support plastic rotation, and finally achieves real blast load distribution.

First method by FEM is the alternate load path method (ALP method) that is mainly advised in the current building design codes and standards in the U.S., including General Services Administration (GSA) [9] and the United States, UFC guidelines [5, 10]. Their methodology takes into account the event-independent dynamic column removal as the main design scenario to evaluate the potential for progressive collapse by transferring loads to members with proper capacity and ductility close to the failed member. Pordel Maragheh et al. [11], Ahmed Galal et al. [12] and Wang et al. [13] discovered that the ALP analysis produces relatively conservative results as it ignores the accidental initial load, potential damage to other structural elements next to the removed columns, and it disregards the structure's non-zero initial conditions (displacement, velocity,

acceleration) before progressive collapse begins, which may result in inaccurate predictions.

The second method is Direct Simulation Monte Carlo method (DSMC method) which is a multiple probability mathematical technique used for simulation explosion details to estimate failure probabilities based on this technique [14]. It is accurate for failure risk and in estimating the likelihood of structural collapse due to blast loads. However, this method is arduous, time consuming to generate many samples to get the desired output especially expensive designed software.

The third common method is the mechanical modelling of the explosive using Jones-Wilkins-Lee model (JWL method) or using one element for explosive by a solid TNT model which is commonly used in hydro simulations to characterize thermodynamics of high explosives. Its application necessitates the fluid-structure interaction, that employs a coupling algorithm [15]. This method can be impractical to apply in the case of very massive structures. Hence, its drawback is the need of discretizing that may lead to multi-physics transient problems so that it is quite pricey and has a wide range of element sizes.

The fourth method is using pressure-time curves by two approaches called compressed- balloon and control-volume method. The compressed-balloon is a phenomenological model based on the pressure-time function resulting from air-compressed balloon [16] or by water-compressed bubble [17]. On the other hand, the control-volume method is based on modelling volume around the explosive that is provided by a pressure-time curve taken from Kingery and Bulmash [2]. The main disadvantage, though, is the computational time in simulation the blast phenomena.

Modeling blast with load-time function that are built with the empirical models by TM5-855-1, TM5-1300 [18], CONWEP [19], A.T.-BLAST [20-23], and EUROPLEXUS [24] is the fifth method for blast simulations by FEM. All previous methods are categorized in Figure 2.

The decision to use which one of these methods is determined by the topic of analysis regarding their advantages and calculation costs. A.T.-BLAST model is approved in the present study to calculate the blast load on the structure. It is computationally efficient using the commercial software A.T.-BLAST that predicts the explosive effects and evaluates potential blast damage [20].

A.T.-BLAST model calculates the blast loading parameters at modified Friedlander's Equation 2 for an open hemispherical explosion as a function of standoff distance, Z and the incidence angle, α_a with a unit value of TNT equivalency factor (inputs). The outputs calculated are the shock front velocity, time of arrival (t_a), pressure (P_s), impulse (I) and duration time or the load duration of blast loading (t_d+). The duration time calculated from this program is called the "The equivalent linear load duration" for the simplified blast load profile

in which the positive phase of the blast's impulse is preserved and the decay of overpressure is supposed to be linear, as shown in previous Figure 1.

(a)   (b)

(c)   (d)

(e)   (f)
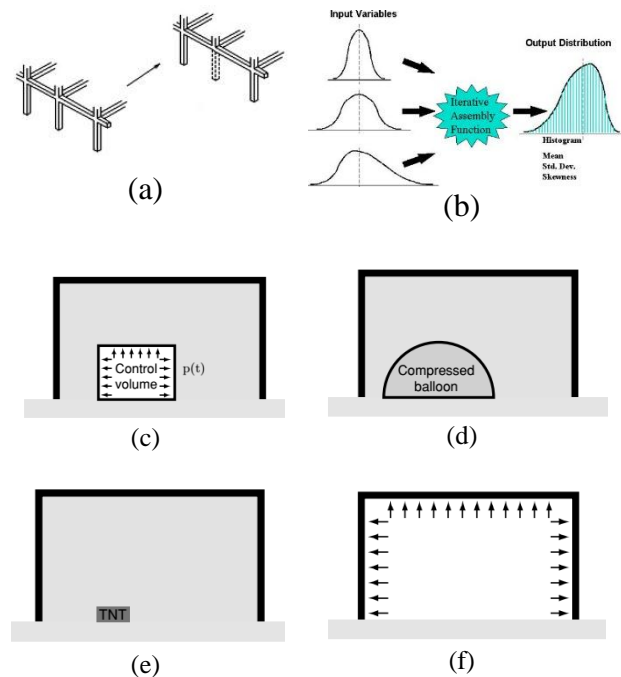
Figure 2: Types of modelling blast loads to structure [16] (a) ALP method (b) Monto- Carlo simulation (c) Pressure time by Control-volume (d) Pressure time from compressed-balloon (e) JWL model or one solid TNT (f) Load-time function by empirical methods

Hence, the ability of the structure to be loaded by a load-time function generated with the pressure-time function by modified Friedlander's equation is a benefit of this model. The common application of load-time function in FEM programs is called "the direct simulation method" which is a threat-dependent methodology that illuminates more properly and realistically the phenomenon of progressive collapse since a structure's damaged area is not restricted to a single structural component, but rather a dispersed damaged area in which the components suffer varying degrees of damage. Best efforts of this method was made by Feng Fu [6, 21] who investigated structure response using the direct simulation of blast load applied directly to the frames and floors of the structure with the calculated parameters of blast wave by using A.T.-BLAST program. And then, each of Bagheripourasil et al. [22], Pourasil et al. [23], Sideri et al. [25], Abdallah et al. [26] and Ahmed Galal et al. [12] also investigated the progressive collapse for steel structure exposed to blast loading the same way and results were accurate in examining the structural response.

Hence, It was the chosen method for this study in modelling blast loads to structures. Steps of methodology are:

3

- Using the simplification of blast wave profile by the equivalent triangular pulse to deduce the pressure time history of blast loading on the structure using A.T.-BLAST model to calculate the blast parameters and the equivalent linear load duration, as shown in Figure 3.

- Then, assuming the blast pressure in ABAQUS/CAE software to be uniformly distributed as an area load operating directly on the slabs and as a line load acting directly on the beams and column face, both width and height.
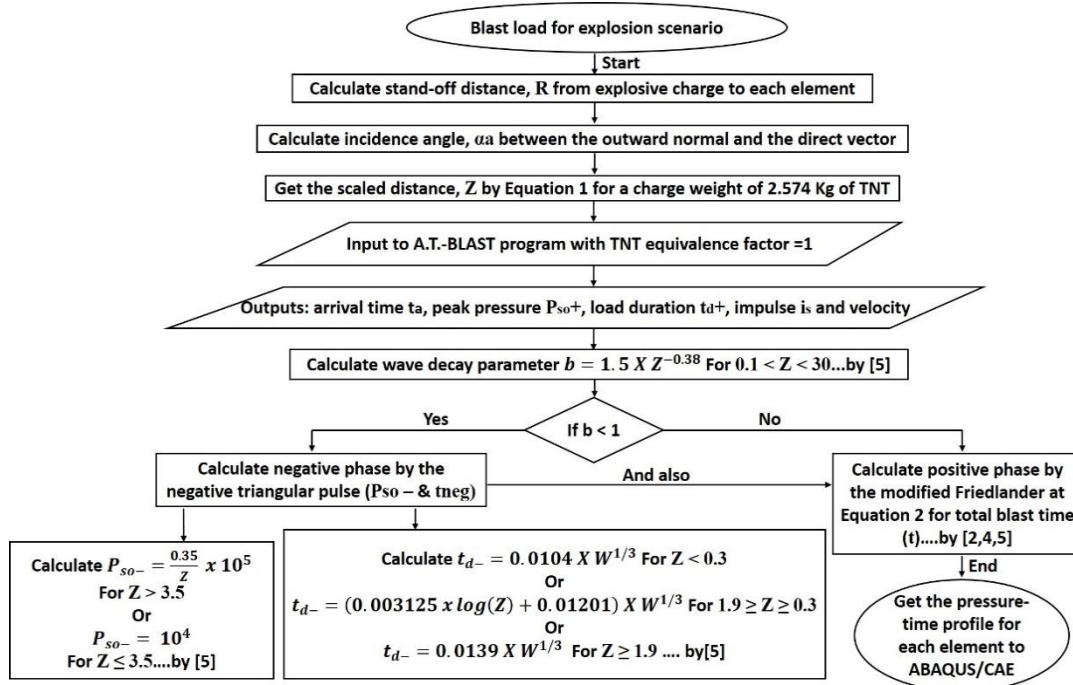
Blast load for explosion scenario

Start

Calculate stand-off distance, R from explosive charge to each element

Calculate incidence angle, αa between the outward normal and the direct vector

Get the scaled distance, Z by Equation 1 for a charge weight of 2.574 Kg of TNT

Input to A.T.-BLAST program with TNT equivalence factor =1

Outputs: arrival time t_a, peak pressure $P_{so}+$, load duration t_d+, impulse i_s and velocity

Calculate wave decay parameter $b = 1.5 \ X \ Z^{-0.38}$ For $0.1 < Z < 30$...by [5]

If b < 1

Yes → Calculate negative phase by the negative triangular pulse ($P_{so}-$ & t_{neg})

And also

No → Calculate positive phase by the modified Friedlander at Equation 2 for total blast time (t)....by [2,4,5]

End

Get the pressure-time profile for each element to ABAQUS/CAE

Calculate $P_{so-} = \frac{0.35}{Z} \ x \ 10^5$ For $Z > 3.5$ Or $P_{so-} = 10^4$ For $Z \leq 3.5$....by [5]

Calculate $t_{d-} = 0.0104 \ X \ W^{1/3}$ For $Z < 0.3$ Or $t_{d-} = (0.003125 \ x \ log(Z) + 0.01201) \ X \ W^{1/3}$ For $1.9 \geq Z \geq 0.3$ Or $t_{d-} = 0.0139 \ X \ W^{1/3}$ For $Z \geq 1.9$ .... by[5]

Figure 3: Blast load profile from A.T.-BLAST program to ABAQUS/CAE program

The primary goal of this research is to provide a rapid blast evaluation and simplify the model by ignoring the influence of blast wave reflections on structural and non-structural members after the explosion when the blast wave is just starting to hit the structure using the direct simulation method by A.T.-BLAST model. At the end of simulation, the original ALP method will be used to check the probable stability of structures after sudden loss of damaged columns.

2. FINITE-ELEMENT MODELING

2.1 Verification of Numerical Model with Experimental Work

2.1.1. Steel Structure Configuration

Direct simulation method using A.T.-BLAST model will be verified using the experimental data provided by Dinu et al. [27] in which a 3D steel frame building consisting of two bays, two spans, and two stories was tested for different blast loading conditions. The structural system is made up of moment resistant frames that run in the x-direction (transvers direction) and braces are introduced in each frame concentrically on the y-direction (longitudinal direction). The design of this structure considers seismic design requirements by using EN 1991-1-7 [28] in which the designed seismic action is low seismicity of a horizontal acceleration equals to 0.10 g. The other permanent loads are dead load of 5 kN/m^2 and live load of 4 kN/m^2 and additional gravity loads with an equivalent value of 7.5 kN/m^2 are positioned on the floors on the first bay.

The steel material in beams, columns, and plates is S275. Cross sections provided in the test were HEB260 for columns, IPE270 for main beams, IPE200 for secondary beams between columns, and IPE180 for intermediate secondary beams. The concrete slabs were 100 mm in thickness of Concrete-Class B40. To evaluate the damage of near-field explosions on the structural elements, eight sensors are used at four different locations to measure blast pressure during test, as shown in Figure 4.
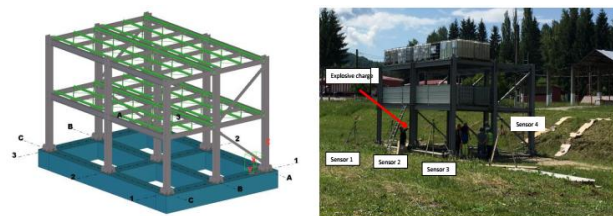

Figure 4: Geometry of the blast test provided [27] showing locations of explosive charge and sensors

According to Table 1 for [27], eight blast tests were performed on the structure. The chosen test for validation in this study is test E6 in which explosive charge equals 2574 g, distance from the front face of the central perimeter column C2 was 200 mm and height of charge from base was 1750 mm.

2.1.2.   Numerical Modelling Technique of Blast Phenomena

Finite element approach was used for modeling the previous steel frame using the ABAQUS/CAE software version 6.14-1 [29]. All steel beams and columns were simulated by 2-node linear wire elements in space (B31), while slabs were described by 4-node shell elements with uniform thickness (S4R). The beam-to-beam and beam-to-column connections were defined using tie nodes that are appropriate for both dynamic and static analyses. Geometry of 3D steel frame before explosion, test E6, is shown in Figure 5.
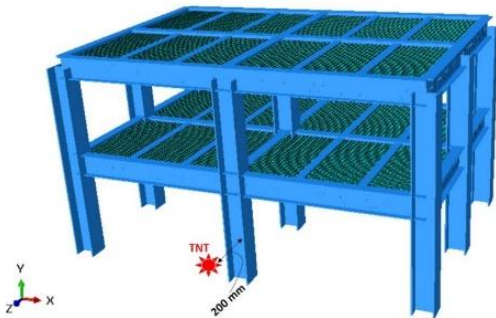
Figure 5: Geometry of the 3D steel frame before explosion test E6 at 200 mm from middle column C2

Application of blast test E6 was performed using Dynamic-Explicit procedure, as shown in Figure 4 for total blast time (t) by 0.005 seconds and each step time for calculation is 0.0005 seconds. An example for the Friedlander waveform calculation for pressure profile is shown at Figure 6 for column C2 at a distance of 200 mm from explosive charge.
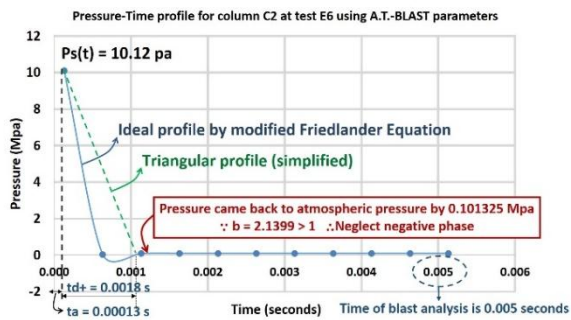

Figure 6: Pressure-Time profile of column C2 at test E6 using A.T.-BLAST parameters

Direct simulation method takes place by transferring blast load profile by A.T.-BLAST into uniformly distributed loads by ABAQUS/CAE so that blast loading is simulated by linear loads on beams, columns face and width, and by area loads at slabs. For test E6, the elements affected by blast were columns at interface, all elements at first story and ground columns, as shown in Figure 6. Effect of slab prevents blast loads reach the second story.
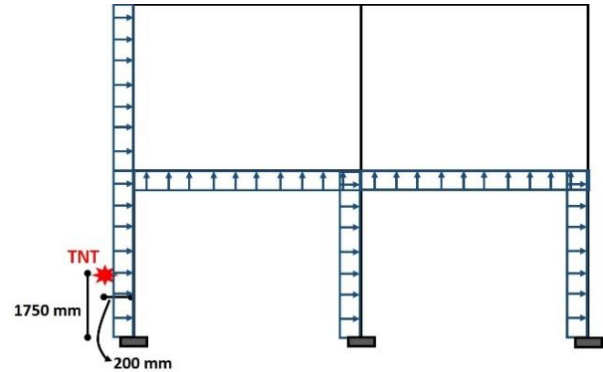

Figure 7: Manner of direct simulation method on structural elements for test E6

2.1.3.   Mechanical Properties of Steel and Concrete under High Strain Rate

Blast loads produces high strain rates in the range of 10^2 to 10^4 s^{-1} more than any other kinds of extra-ordinary hazards, as shown in Table 1 by [30, 31]. Hence, these high straining rate results in increasing yield stress and ultimate strength of steel due to high-rated deformations. As its ultimate elongation decreases, modulus of elasticity (under high strain rate) remains constant. In concrete, both compressive and tensile strength increase and the tensile strength can increase as much as 6 to 8 times of its static compressive strength [32].

According to the numerical modal calibration provided by the experimental study, the chosen model for S275 steel was the bilinear strain-hardening (isotropic elastic-strain hardening) model as the strains during blast reaches the strain hardening range by the ultimate strain when the component fractured. On the other hand, during explosions, strengths exceed their minimum requirements so that the design materials strengths should be raised by a Strength Increase Factor or Dynamic Increase Factor (DIF) to obtain realistic properties for steel under high strain rate of blast. The bilinear model is shown in Table 2 by [33] with value of DIF by 1.1 according to SCI guideline [7] for S275.

Table 1. Several strain rates of extra-ordinary hazards by [30, 31]

Load Features	Blast Load	Cyclone	Earthquake	Persistent Wind	Floods
Forcing Function	P (R, W), I(R, W)	P (wind speed v_2, ρ)	Force F (mass m, acceleration a)	P (wind speed v_2, ρ)	F (flow rate Q_2, contact area A, ρ)
Duration	Milliseconds	Seconds		Hours	
Loading Time History	Exponential	Random	Combined sinusoidals	Random	Sinusoidal
Damage on Structure	Localized	Global			
Loading Regime	Impulsive or Dynamic	Dynamic		Quasi-static	

The chosen model for concrete material was the simplified concrete damage plasticity model (CDP model) was developed in ABAQUS/CAE for this analysis according to concrete class B40 by [34], in which the hardening and softening variables are used to determine the cracking and crushing trends. The assumptions of this model were: plastic flow was unassociated, different description of compression and tensile behavior of concrete, damage parameters, individually for tension and compression to allow reduction of material stiffness, two damage mechanisms: cracking and compressive crushing of concrete and finally model values are derived from the laboratory tests by uniaxial compression and tension, the bi-axial failure test and tri-axial test.

Due to the high strain rate of concrete at extra-ordinary events like explosions, concrete's unconfined compressive strength increases with loading rate so that using the Strength Increase Factor or Dynamic Increase Factor (DIF), which is dependent on the strain rate, is a must to increase the dynamic ultimate strength significantly larger than the static ultimate strength. Hence, the used value for increasing compressive strength of concrete B40 is 1.25 according SCI guideline [7] and GSA guideline [9], as shown in Figure 8.

Table 2. Modeling bilinear strain-hardening of steel S275 model in FEM by [33]

| Bilinear strain-hardening model of S275	
Density (Kg/m3)	7800
Elasticity modules (GPa)	200
Ultimate stress (MPa)	270
Poisson's ratio	0.3
Plastic strain failure	0.36
DIF (dynamic increase factor)	1.10

(a)

(b)

Figure 8: Values for DIF of concrete as provided in guidelines (a) at GSA (b) at SCI

#### 2.1.4. Verification of Numerical Model with E6 Test Results

As shown in Figure 7, results have shown good agreement between experimental data and the FEM simulation using direct simulation method by A.T.-BLAST model. Figure 9 (a) shows the values of pressure at sensor 1 at test E6 that is calculated using A.T.-BLAST program by Friedlander waveform within 0.005 seconds. Figure 9 (b) shows the values of pressure with stand-off distance for each element subjected to explosive charge by test E6. While Figure 9 (c) shows the values of vertical displacements of perimeter beams from the first floor (C1-2 and C2-3) after removing the central column C2 at distance 4.5 m. Finally, Figure 9 (d) shows the values of strain with time in the web of the central column C2 at top side of the column (T15) and at bottom side of the column (T13).
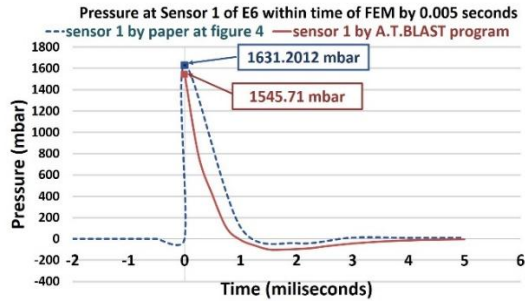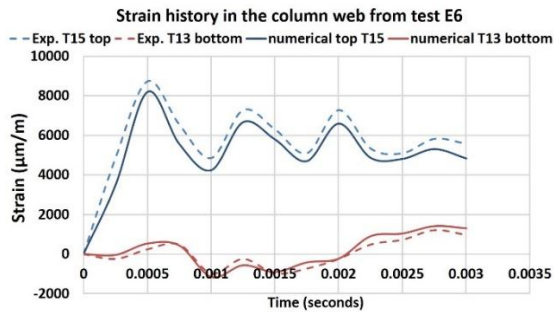
(a)
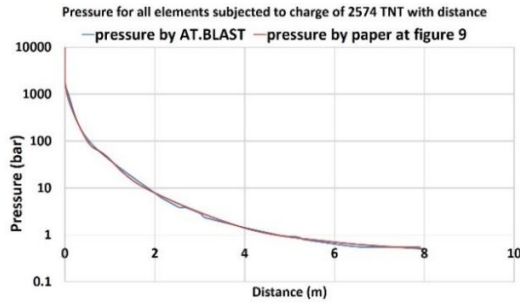
(b)
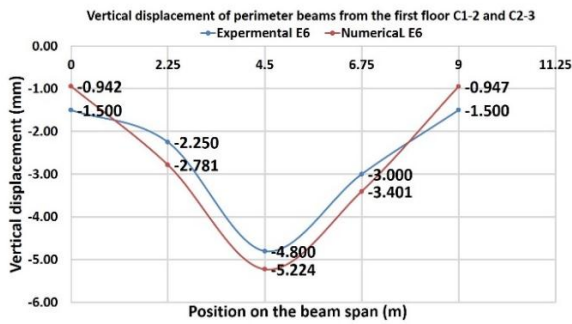
(c)

(d)

Figure 9: Calibration with experimental results by test E6 (a) pressure at sensor 1 using A.T.-BLAST model (b) pressure with stand-off distance for each element subjected to explosive charge (c) vertical displacements of perimeter beams (d) strain history in the web of the central column C2

2.2 Case study of a low-rise structure subjected to external explosion

The chosen structure for the case study was a 3-story steel composite frame factory that was designed according to American Institute of Steel Construction (AISC) requirements [35]. The structural plan is 35.5 x 50 m^2.

2.2.1. Structural configuration

The 3D steel–concrete composite structure is comprised of three stories each with a uniform story height of 6.00 m. In the long direction, there are seven bays spanning 6.50 m in the first bay, 7.50 m in the next five bays, and 6.00 m in the last bay, in addition to five bays in the short direction, spanning 7.10 m each. Moment-resistant frames are all frames in the y direction and only the perimeter frames in the x direction. The secondary beams for the two stories are parallel with the perimeter moment-frame in the short side direction, and at each story level, a 100-mm RC slab is joined to the skeleton steel frame. The slab is reinforced in both directions with ASTM A615 Grade 40 reinforcing mesh of minimum-shrinkage rebars R10 @ C-C 200 (10 mm diameter, bar spacing 200 mm center-to-center) with a 25-mm cover. All steel sections are AISC W-shaped, with W18x11x158 columns, W24x12.75x229 main beams of frame at first story, and W14x16x665 for all secondary beams and main beams of frame at second story. The roof consists of slope beams at 1:10 are of the same section as columns and purlins of Z-section 200 of 15 mm thickness and corrugated sheet steel of double layer is 16 mm thickness. The system is braced by vertical and horizontal bracing of two angle back-to-back 2L89×89×7.9. Cross sections are provided at Table 3.

Table 3. Cross section of steel frame of case study according to AISC requirements

Section by AISC	Height (d) mm	Width (b) mm	Flange thick. (t_f) mm	Web thick. (t_w) mm
Columns & slope beams W 18X11X158	501	287	36.6	20.6
Main Beams 1st floor W24X12.75X229	661	333	43.9	24.4
Sec. Beams & Main Beams 2nd floor W14X16X665	550	448	115	71.9
Bracing 2L 89x89x7.9	88.9	88.9	7.9	7.9

The loads acting on the structure consists of gravity loads, dead loads, live loads and wind loads. Gravity loads which are the self-weight of all the structure were considered, Dead loads were 0.15 kN/m^2 for steel sheet at roof and 3 kN/m^2 for first and second floor, live loads were 0.57 kN/m^2 for roof, 7.5 kN/m^2 for first floor and 3 kN/m^2 for second floor. Wind loads were calculated

7

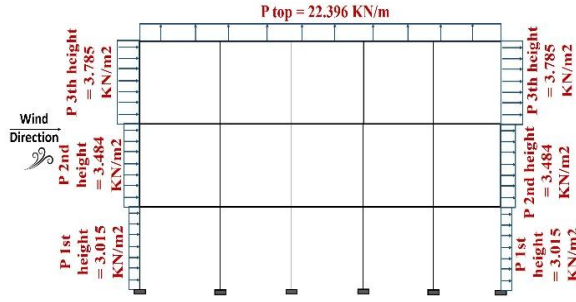according to wind speed of 130 km/ph, as shown in Figure 10.

Figure 10: Wind loads calculations on structure according to ASCE requirements.

2.2.2. Numerical Modelling Technique of Blast Phenomena

Because of the complexity of the modeling, some simplifications have been considered in the analysis such as the slope of third story and simulating the structure using wire and shell elements, instead of the solid elements to decrease the time required to complete the analysis.

Steel beams and columns were modelled using 2-node linear wire elements in space (B31), while slabs were defined using 4-node doubly curved shell elements with uniform thickness (S4R). The choice of element type determines the accuracy of the results so that the free triangle with mapped meshing for finite membrane strain was chosen for simplicity and computational efficiency. Tie nodes were used to describe the beam-to-beam and beam-to-column connections, which was adequate for both static and dynamic analysis.

The 3D view of the structure geometry is shown in Figure 11 (a), side view and elevation of the frame with levels at (b) and (c) and key names of columns are shown in Figure 11 (d).
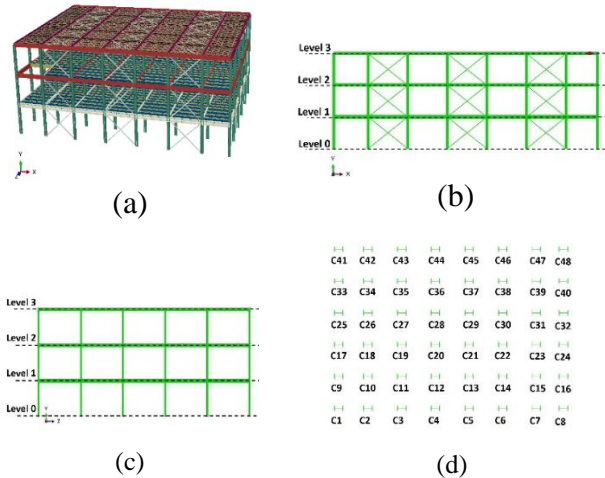

Figure 11: Structure view using ABAQUS/CAE (a) the 3D geometry (b) side view (c) end gable of structure (d) key names of columns.

2.2.3. Material model of steel and concrete at high strain rate

The simplified concrete damage plasticity model (CDP model) was also chosen for modelling the dynamic behavior of concrete material under blast loading in FEM under high strain rate according to concrete class B40, taking into account the dynamic increase factor (DIF) by 1.25.

For all steel parts of columns and beams, the chosen constitutive hardening model to consider the strain rate effect is the strain rate dependent Johnson-Cook (J-C) model for mild steel of grade ASTM A36. It is a strength model based on several experiments by Johnson-Cook [36] to characterize the mechanical properties of metal materials that undergo high-rated deformation or melting process as a result of blast loading at high temperatures. The main material responses in this model are strain-rate effects, strain hardening, and thermal softening and are combined in a multiplicative manner in Equation 3:

$$\sigma_y = \left(A + B \left(\varepsilon_{eff}^p \right)^N \right) \left(1 + C \ln \dot{\varepsilon} \right) \left[1 - (T_h)^M \right] \quad (3)$$

Where, the first part is the effective plastic strain ε_{eff}^p to determine the elastic yield stress A, the second part is the strain-rate hardening $\dot{\varepsilon}$ to determine A, B and N and the last part includes the stress softening caused by high temperature. Parameters B, N, C and M are control material parameters that determined using quasi-static tensile tests and bar tests. The material failure is a subset of the ductile criterion. Hence, the equivalent plastic strain occurs at the onset of damage or fracture when the damage parameter D approaches 1.0 by a damage-accumulated criteria assumed in a linear way [36]. The final equation for failure is:

$$\varepsilon^F = \left[D_1 + D_2 + \exp \left(D_3 \frac{P}{\sigma_{eff}} \right) \right] \left(1 + D_4 \ln \dot{\varepsilon} \right) + D_5 T_h \quad (4)$$

Where, D_1 to D_5 are material constants, P is the mean stress and ε_p is the strain rate at the failure limit.

The main advantage of this model is treating temperature and strain rate effects as the use of the isotropic hardening model may result in higher stresses and strains. The J-C model is embedded in ABAQUS/CAE program to calculate the flow stress by combining the plastic strain hardening, strain rate, and temperature terms. The properties of J-C model of A36 and the failure model for steel A36 are provided by [26] with a Dynamic Increase factor (DIF) by 1.1 according to SCI guideline as well.

On the other hand, the dynamic behavior of reinforcement ASTM A615 Grade 40 for concrete slabs is defined under blast loading in FEM using the bilinear strain-hardening (isotropic elastic-strain hardening) model and this reinforcement is embedded in the shell element in smeared layers available in ABAQUS/CAE. The properties of bilinear model of rebar A615 is provided by [22].

Two-Stage Structural Analysis

2.2.4.   First stage: Determination of blast loading using Direct Simulation method

The structure is subjected to an external explosion by 0.25 ton charge of TNT with a standoff distance of 4.00 m from Column C4, which can be carried by a package bomb that is selected as this form of attack is more difficult to resist than other attack scenarios such as vehicle bombs, as shown in Figure 12. Blast parameters for Column C4 (level 0-1) and slab 6 (level 1), as an example, are listed in Table 4 and their deduced pressure-time curves are shown in Figure 13.

As shown in previous Figure 3, the application of blast loading on structural elements is simulated by Direct simulation method using the empirical model by A.T.-BLAST program, as shown in Figure 8. The explosion duration was standardized to be 0.5 seconds to allow the pressure wave to reach the parts far from charge along the structure. The time consists of two steps:

- First step time is taken by 0.2 seconds with incremental time of 0.005 seconds for positive phase of blast loading (for all elements subjected to explosions).
- Second step time is taken by 0.3 seconds with incremental time of 0.001 seconds for negative phase of blast loading (added to elements forming negative phase after reaching atmospheric pressure).
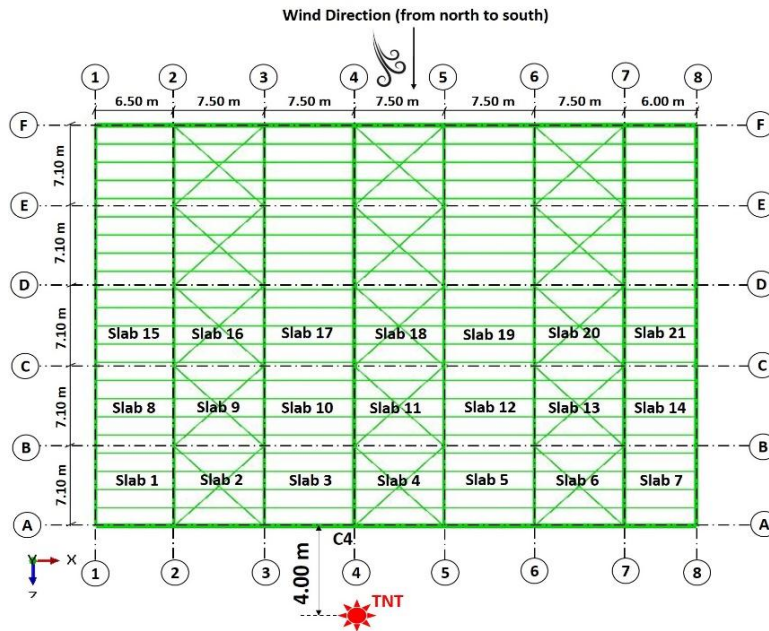

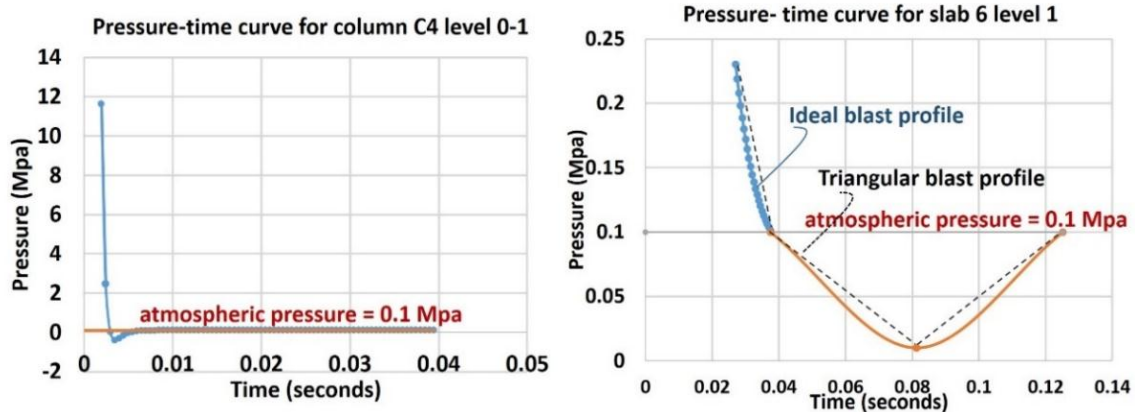**Figure 12: Position of external explosive charge relative to structure**

Figure 13: Pressure-Time curve for Column C4 (level 0-1) and slab 6 (level 1)

Table 4. Calculations of blast parameters for some elements

Chosen element	Column C4 level 0-1	Slab 6 level 1
Stand-off distance, R (m)	5.00	21.09
Incidence angle, α_a (deg.)	36.871°	73.467°
Charge weight, W_{TNT} (ton)	0.25 TNT	0.25 TNT
Peak positive overpressure, $P_{so}+$ (Mpa)	11.63217	0.23024
Equivalent linear load duration, t_d+ (sec.)	0.00096	0.0107
Wave decay parameter, b	1.6377 > 1	0.9478 < 1
Peak negative pressure, $P_{so}-$ (Mpa)	------	0.01
Negative duration, t_d- (sec.)	------	0.08757
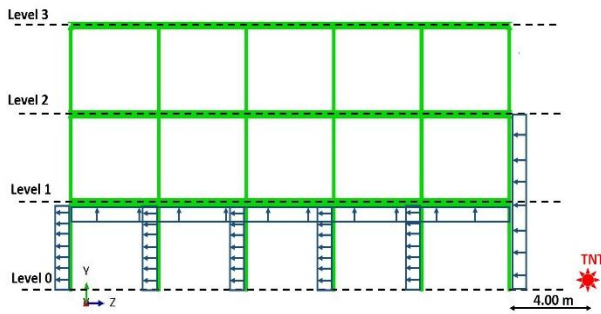
Figure 14: Direct simulation method on structural elements of the case study

2.2.5. Second stage: Structure re-loading after explosion by ALP method with heat effect

In order to evaluate the damage after explosion by examining the stability of the structure, the Alternate Load Path method (ALP) was used in the static analysis by removing the columns that had been damaged due to the effect of external explosion (all key columns). Evaluation of stability is deduced by reloading the structure with the sudden loss of these columns to resist the initial loading before explosion such as dead, live, and wind loads in the elastic-static condition. Hence, loads are transferred to the members adjacent to the failed columns that have sufficient capacity and ductility. This stage will provide an indicator of the structure's overall stability to identify if it is usable or can be repaired by its damage class or the explosion have resulted in a complete destruction.

A new additional temperature load was applied after the scenario of explosion to only the adjacent elements to the removed columns by ALP method. Simulating the heat effect was performed using the fire curve that was developed by the ISO 834 [37] which is a temperature-time curve that shows the gradual change of temperature over time to indicate the condition of the structure after explosion [11]. The equation of such curve is applied to the adjacent members of the removed columns, as below by:

$$T = T_o + Log_{10} \left(8\,t + 1 \right) \tag{5}$$

Where, T_o is the initial temperature of TNT that equals to 3100 °C and t is the time of analysis. The load sequences for first and second stage after explosion by ALP method is shown in Figure 15.

2.2.6. Load combinations according to guidelines SCI, UFC, and GSA.

The analysis of external explosion in this study is based on load combinations and damage criteria from three of the general design manuals and computational approaches in forecasting blast loads and the responses of structural systems. These standards were designed specifically for military purposes. However, their knowledge applicable to civil design applications.

The load combinations for first stage by explosions and second stage after explosion by ALP method is provided in Table 5. In addition, due to the limited data on wind in blast guidelines, the lateral wind load is factored by 1.00 in all guidelines, except for ALP methods in UFC, it is factored by 0.2 [38].

Table 5. Load combinations for first and second stage of loading

| Guideline	Load combinations at first stage (during explosion by Direct Simulation method) Dynamic analysis	Load combinations at second stage (after explosion by ALP method) Static analysis
SCI guideline [7]	1.0 D.L + 1.0 L.L + 1.0 Wind + 1.0 Blast	1.0 D.L + 1.0 L.L + 1.0 Wind
UFC guidelines [5, 10]	1.2 D.L + 0.5 L.L + 1.0 Wind + 1.0 Blast	Near to charge: $\Omega_N(1.2$ D.L + 0.5 L.L$)$ + 0.2 Wind, $\Omega_N = 2$ Far from charge: 1.2 D.L + 0.5 L.L + 0.2 Wind
GSA guideline [9]	1.0 D.L + 0.25 L.L + 1.0 Wind + 1.0 Blast	2(1.0 D.L + 0.25 L.L) + 1.0 Wind
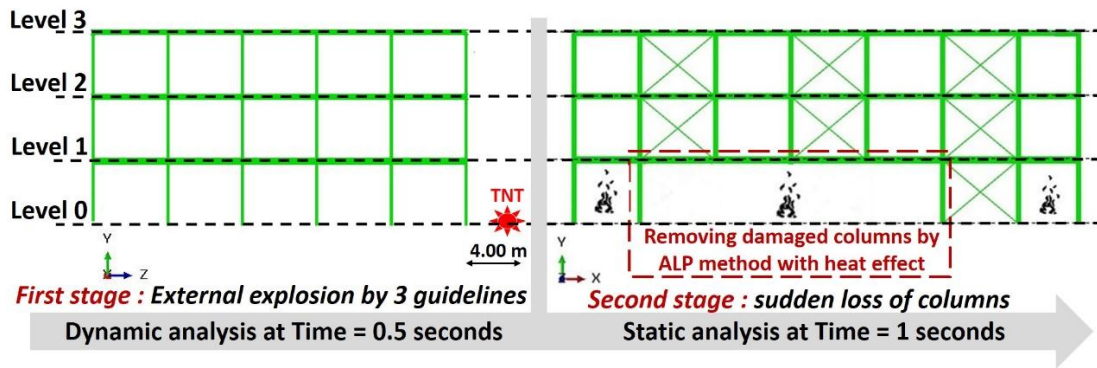
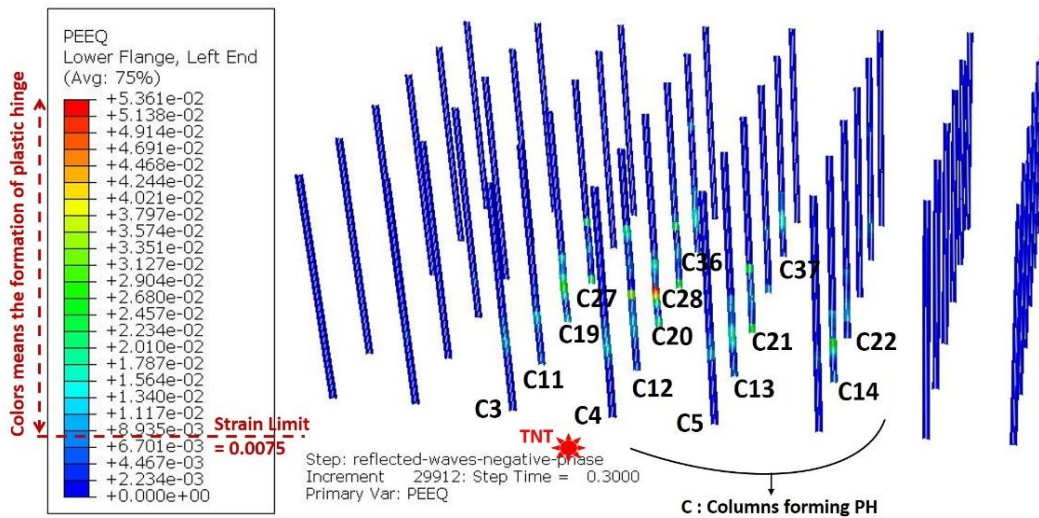**Figure 15: Load sequences for first and second stage**

Figure 16: Fifteen columns forming plastic hinge at end time of 0.5 seconds by SCI guideline

2.3 Analysis Results

2.3.1. Damage assessment of columns

The general failure modes of columns subjected to explosions; are overall buckling that occurs under combined axial compression and bi-axial bending, local buckling that occurs under axial strain and lateral blast pressure, distortion of cross section that occurs due to blast pressures resulting in folding of flanges and dishing of web, shear failure of column ends that occurs under primarily the combined effects of shear and bending, fracture of tension flange that is more possible for columns with small axial compressive load or those with tension uplift, failure of column splices that occurs under combined bending, shear and possible uplift, failure of base plate/ anchor bolts assembly that occurs primarily under shear effects and possible uplift due to blast loading and finally fracture of foundations more likely for spreads footings without piles and those with small axial compressive load or with tension uplift [30].

Hence, columns fail due to one or more of these modes due to explosion, and this study concentrates on the main causes of failure to columns due to moment

(forming plastic hinges), shear or axial load (compression by buckling or tension by uplift).

After the explosive detonation, the high-pressure pulse generates a compressive stress wave on the element's face that creates rapid changes in the structure's strain field. Figure 16 (using SCI guideline) shows the failure of about 15 columns by high equivalent strain due to the initial formation of plastic hinges (the same for UFC and GSA guidelines). For other columns located far from the blast charge, there is no evidence of plastic strain (Blue columns, PEEQ = 0). This indicted that the column's yielding is only limited to a small area within the building. Knowing that, PEEQ is a scalar variable indicating the material's inelastic deformation. If this variable is greater than zero, the material has yielded. For this material model, values greater than 0.0075 represents a fracture or plastic hinge failure.

An example for plastic strain (PE11) (axial strain for column) at different locations of column C20 level 0-1 by SCI guideline is chosen to be illustrated at different locations at time intervals (0, 0.05 ,0.1 ,0.15 ,0.2 ,0.25 ,0.3 ,0.35 ,0.4 , 0.45 , 0.5) till end of explosion. It reaches the maximum value at mid height, where plastic hinge forms (H= 3.00 m) all over time to attain 0.039602 at

11

negative direction, as shown in Figure 9. However, the strain values of both locations at 1.50 m and 4.50 m of the column are within the limit.
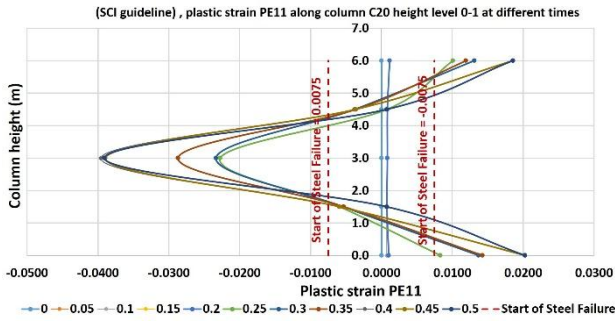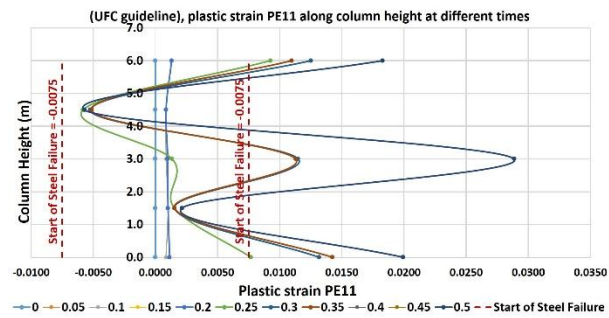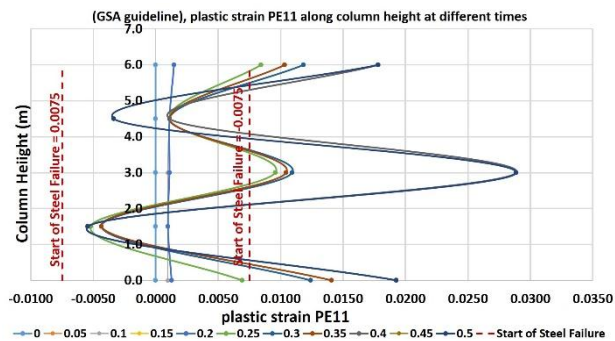

Figure 17: Plastic strain (PE11) of column C20 (level 0-1) at different locations with time intervals by SCI guideline

On the other hand by UFC and GSA guidelines at Figure 10, plastic strain reaches the maximum value at mid height by 0.028864 and 0.028863 at positive direction, respectively due to live load reduction. Hence, SCI guideline is overestimated for evaluation plastic strains PE11 at different locations of column height.

(a)

(b)

Figure 18: Plastic strain (PE11) of column C20 (level 0-1) at different locations with time intervals (a) by UFC guideline (b) by GSA guideline

Figure 19 shows the combined curve for maximum values at each location of this column based on the three guidelines, each in their own direction. Therefore, effect of live load on the maximum absolute values of plastic strain PE11 values at mid height of column C20 level 0-1

appears in the following lines; when the live load is increased by 300% from GSA to SCI, the absolute PE11 value increases by 37.207 %. However, increasing live load by 100 % from UFC to SCI has no effect on the plastic strain value and remains constant. In a word, curve by SCI guideline of total value of live load has provided the greatest absolute values of plastic strain while curves by UFC and GSA guidelines are the least.
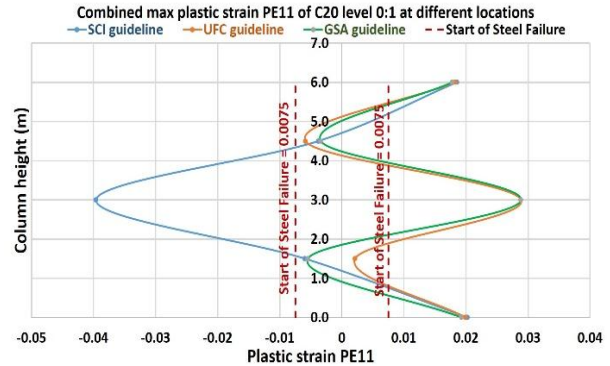

Figure 19: Combined curve of plastic strain PE11 of column C20 level 0-1 at different locations according to the three guidelines

Due to the behavior of steel under high strain rate, the substantial rise in the yield stress during blast has important ramifications for steel structures as it increases considerably while the ultimate strength increases only with a small amount. To represent the relationship between stress and plastic strain at plastic hinge, equivalent plastic strain (PEEQ option in ABAQUS/CAE) is used. Hence, Figure 20 represents the behavior of initial formation of plastic hinge of Column C20 level 0.5 at plasticity region after yielding till failure.

The ultimate stress after yielding at 270 MPa (point 1) starts to increase immediately to reach point 2 within 0.2 seconds from start of explosion with a corresponding value of equivalent plastic strain that is less than the strain limit. Passing from point 2 towards point 3, the plastic strain exceeds the plastic limit of 0.0075 by stress greater than yield at time 0.260008 seconds (point 3) to form plastic hinge at level 0.5 due to high strain while stresses remain constant from point 3 till the end, and hence rotations can increase. Combination between guidelines has proved that they are somewhat identical as there is no effect of reduction or increase of live load at the position of plastic hinge of the column subjected to explosion after yielding as its material is about to fail by increasing stress and strain.
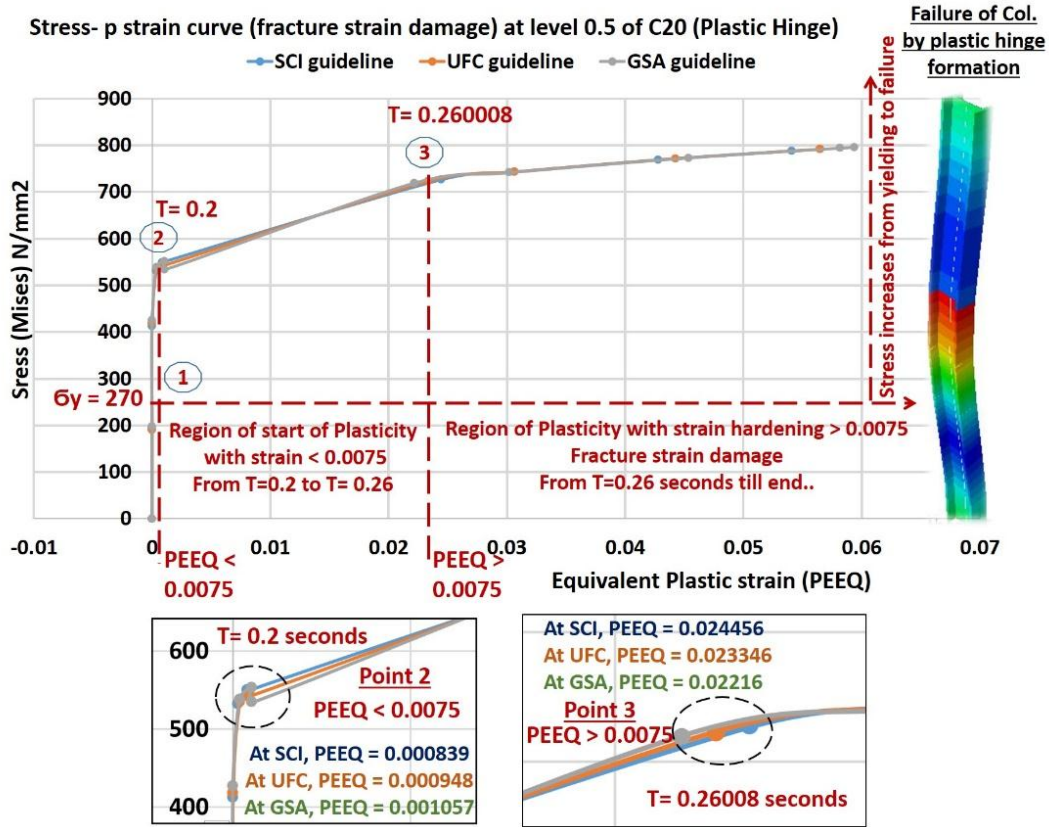
Figure 20: Combined stress plastic-strain curve at level 0.5 of column C20 according to guidelines SCI, UFC, and GSA

Increasing the displacement of a column with sudden change in shape (deformation) under load is considered a buckling failure mode. If the deformations that happened after buckling did not force the member to completely collapse, the member will continue to maintain the load that causes it to buckle; nevertheless, when deformations cause the creation of first plastic hinge, the member is about to collapse by the time.

As shown in Figure 21, the maximum displacement at mid height was 367.882 mm within 0.365 seconds for SCI guideline while it was 361.238 mm for UFC guideline and 352.572 mm for GSA guideline at the same time. So, when the live load is increased by 100 % from UFC to SCI, the maximum value of displacement has increased at mid height by 1.839 % within 0.365 seconds and with the continued increase of live load by 300 % from GSA to SCI, the value has increased by 4.342 % within the same time, so the SCI guideline has provided the greatest values while GSA guideline was the least.

Another important judged acceptability in blast design and evaluation of columns is the capability of columns to resist its internal forces (bending moment, shear force, and axial force). Column C4 that was subjected directly to the explosive charge is chosen for assessment of its internal forces along its height from level 0 to level 1.

Figure 22 shows the bending moment for column C4 at different heights from level 0 to level 1 according to

SCI guideline, with a maximum value at level 1 in 0.15 seconds. In addition, Figure 23 shows the shear force for it according to UFC guideline, with a maximum value at level 0 within the same duration time.
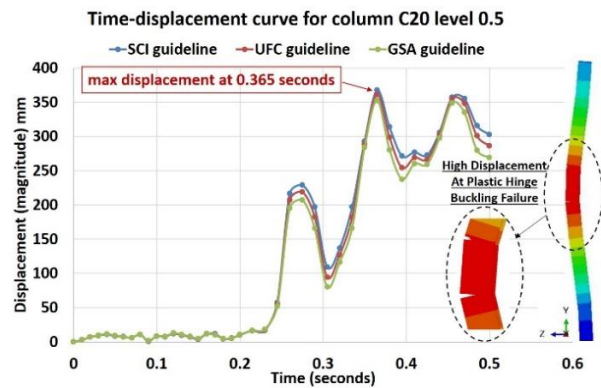

Figure 21: Displacement at mid height of column C20 at level 0.5 according to the guidelines SCI, UFC, and GSA
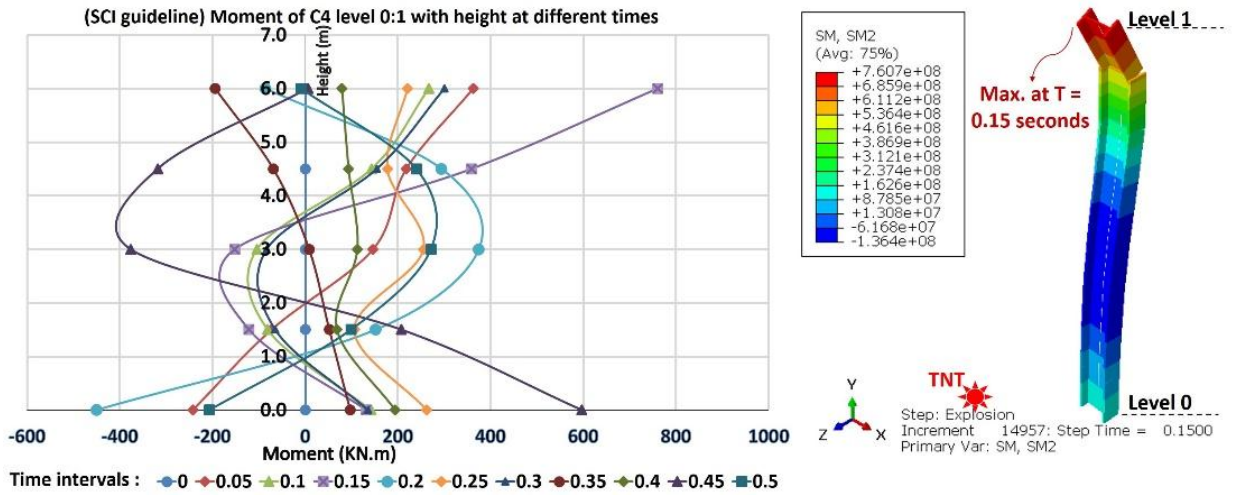
Figure 22: Bending moment for column C4 by SCI guideline along level 0-1
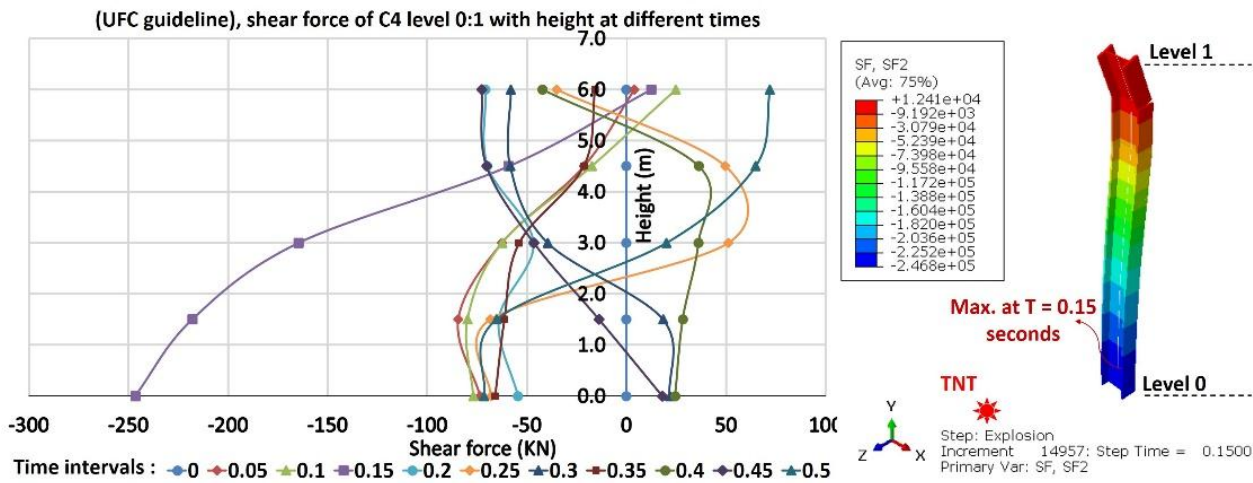

Figure 23: Shear force for column C4 by UFC guideline along level 0-1

The following Table 6 presents value, position and time of maximum bending moment for selected columns according to guidelines. It can be noticed that columns (C20, level 0-1) and (C4, level 0-2) have recorded the highest bending moment values of all. In addition, the closest column C4 has reached the maximum value by only 0.15 seconds but the farther column C20 has reached its maximum value later at 0.35 seconds.

On the other hand, when identifying the effect of live load on maximum bending moment values for columns C4 and C20, it is observed that when increasing live load by 100 % from UFC to SCI for column (C4, level 0-1), the value has decreased by 2.712 % within 0.15 seconds at level 1 and with the continued increase of live load by 300 % from GSA to SCI, the value has decreased slightly by 0.862 % within the same time. In addition, when the live load is increased by 100 % from UFC to SCI for column (C20, level 0-1), the value has decreased by 0.659 % within 0.35 seconds at level 0.5. And with the continued increase of live load by 300 % from GSA to SCI, the value has decreased by 1.20 % within the same time.

As well, the following Table 7 presents value, position and time of maximum shear forces for selected columns according to guidelines. It can be noticed that each of column C2 and C4 have recorded the highest shear force values of all.

On the other hand, when identifying the effect of live load on maximum shear force values for column C2 and C4, it is observed that when increasing live load by 100 % from UFC to SCI for column (C2, level 1-2), the value has decreased by 2.461 % at level 2 within 0.25 seconds. And with the continued increase of live load by 300 % from GSA to SCI, the value has decreased by 4.474 % within the same time. In addition, when the live load is increased by 100 % from UFC to SCI for column (C4, level 0-1), the value has decreased by 0.640 % at level 0 within 0.15 seconds. And with the continued increase of live load by 300 % from GSA to SCI, the value has decreased by 1.502 % within the same time.

14

Table 6. Maximum bending moments for columns according to guidelines by SCI, UFC and GSA

Column	Due to SCI guideline			Due to UFC guidelines			Due to GSA guideline		
	M	**P**	**T**	**M**	**P**	**T**	**M**	**P**	**T**
C2 level 1:2	-592	Level 1	0.05	-602	Level 1	0.05	-610	Level 1	0.05
C4 level 0:1	761	Level 1	0.15	776	Level 1	0.15	790	Level 1	0.15
C4 level 1:2	-797	Level 1	0.15	-811	Level 1	0.15	-823	Level 1	0.15
C6 level 0:1	638	Level 1	0.05	647	Level 1	0.05	654	Level 1	0.05
C6 level 1:2	756	Level 1	0.05	-764	Level 1	0.05	-770	Level 1	0.05
C8 level 0:1	437	Level 3/4	0.05	-311	Level 1	0.25	-308	Level 1	0.25
C8 level 1:2	344	Level 1	0.25	338	Level 1	0.25	333	Level 1	0.25
C15 level 0:1	308	Level 0	0.5	311	Level 0	0.5	317	Level 0	0.5
C20 level 0:1	-1037	Level 1/2	0.35	-1044	Level 1/2	0.35	-1049	Level 1/2	0.35
C21 level 1:2	290	Level 1	0.5	288	Level 1	0.4	290	Level 1	0.4
C28 level 1:2	-558	Level 1	0.4	590	Level 1	0.35	-616	Level 1	0.35
C29 level 0:1	-608	Level 0	0.4	594	Level 1/2	0.4	564	Level 1/2	0.4

* **M**: Value of max moment (kN.m), **P**: position of max bending moment and **T**: Time of max moment (seconds)

Table 7. Maximum shear forces for columns according to guidelines by SCI, UFC and GSA

Column	Due to SCI guideline			Due to UFC guidelines			Due to GSA guideline		
	Q	**P**	**T**	**Q**	**P**	**T**	**Q**	**P**	**T**
C2 level 1:2	332	Level 2	0.25	341	Level 2	0.25	348	Level 2	0.25
C4 level 0:1	-245	Level 0	0.15	-247	Level 0	0.15	-249	Level 0	0.15
C4 level 1:2	-175	Level 2	0.15	-171	Level 2	0.15	-167	Level 2	0.15
C6 level 0:1	-279	Level 0	0.05	-275	Level 0	0.05	-274	Level 0	0.05
C6 level 1:2	188	Level 1	0.2	185	Level 1	0.2	180	Level 1	0.2
C8 level 0:1	-208	Level 0	0.1	226	Level 0	0.25	224	Level 0	0.25
C8 level 1:2	216	Level 2	0.4	213	Level 2	0.4	213	Level 2	0.4
C15 level 0:1	179	Level 0	0.4	166	Level 0	0.4	157	Level 0	0.4
C20 level 0:1	145	Level 1	0.5	-151	Level 1	0.35	120	Level 1	0.5
C21 level 1:2	-193	Level 1	0.4	189	Level 1	0.4	228	Level 1	0.45
C28 level 1:2	124	Level 2	0.25	119	Level 2	0.25	115	Level 2	0.4
C29 level 0:1	140	Level 0	0.25	142	Level 0	0.25	146	Level 0	0.25

* **Q**: Value of max moment (kN), **P**: position of max shear force and **T**: Time of max shear (seconds)
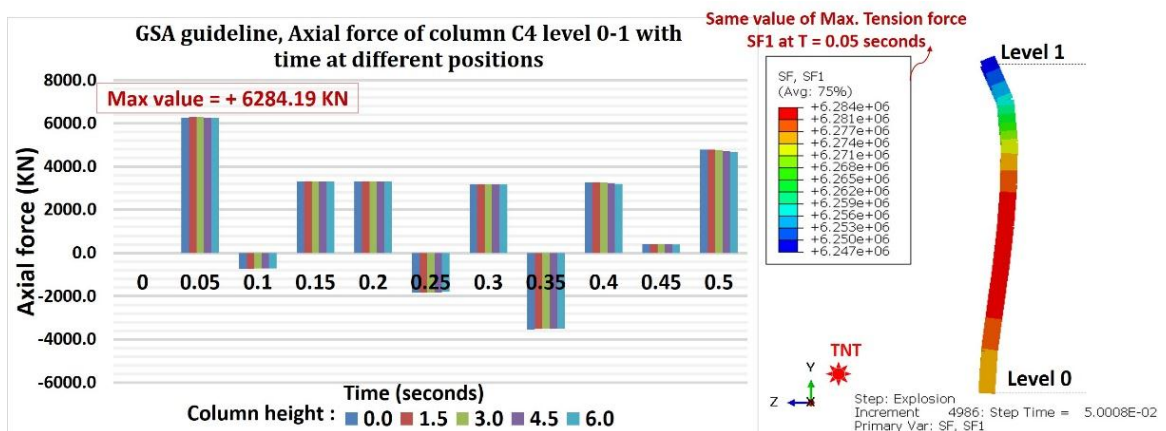
Figure 24: Axial force for column C4 level 0-1 by GSA guideline

As for the axial force, Figure 24 shows the axial force for column C4 at different heights from level 0 to level 1 by GSA guideline and it has reached its maximum tension value by 6284.19 kN within 0.05 seconds. Tension force is common as floor systems lift under blast load so that column C4 exposed to a tension load will fail if the applied tension load causes an internal stress in the member that is greater than the tensile strength of the material (270 Mpa).

The applied stress is calculated by dividing the axial tension force by the cross sectional area of the column (6284190/29821.08 = 210.729 Mpa) so that it is about to fail due to tension stress by the time after explosion (for t > 0.5 seconds). As a result, the cross section of the column begins to elongate and diminish or neck until the column is completely pulled apart into two pieces by combined failure modes (buckling, necking, and shear tearing).

Table 8. Columns of maximum axial force in compression > (P_{cr} = 1617.1274 kN) by guidelines

Column	Due to SCI P_{design} (kN)	Due to UFC P_{design} (kN)	Due to GSA P_{design} (kN)	Comment F
C2 level 1:2	-2837.8	-2783.7	-2728.3	P > P_{cr} in all guidelines
C4 level 0:1	-------	-------	-------	Tension is the max
C4 level 1:2	-2401.3	-------	-------	P > P_{cr} in SCI
C6 level 0:1	-------	-------	-------	Tension is the max
C6 level 1:2	-2389.4	-2133.1	-1896.8	P > P_{cr} in all guidelines
C8 level 0:1	-3995.6	-3928.5	-3868.9	
C8 level 1:2	-------	-------	-------	Tension is the max
C15 level 0:1	-16220.1	-16086.3	-15954.4	
C20 level 0:1	-16819.8	-16860.6	-16920.5	
C21 level 1:2	-14138.2	-14302.3	-14349.5	P > P_{cr} in all guidelines
C28 level 1:2	-15331.8	-15649.5	-15900.7	
C29 level 0:1	-16295.0	-16233.5	-16170.7	

* P_{design}: Value of max compression force (kN) and **F**: Failure at the max value (buckling or tension).

In contrast for the compression axial force, a simplified check of failure due to buckling can be done by using Euler's buckling equation [39]. Equation 6 is not intended for actual design work, but only as a way to illustrate process during high explosion.

$$(P_{design} = axial\ compression\ force) < (P_{cr} = \pi^2\ E\ I\ /\ L_{eff}^{\ 2})\ (6)$$

Where, P_{design} is the column design load, P_{cr} is the critical buckling load, L_{eff} is the effective length of the column, E is elastic modulus, and I is minimum moment of inertia of the cross section of the column about x or y direction. Hence, P_{cr} equals to 1617.1274 kN which is less than all values of axial compression of columns under blast loads and buckling is prevalent. Table 8 lists the most affected columns with their loads according to the three design guidelines.

2.3.2. Damage assessment of slabs
As soon as the explosion has taken place, the distribution of pressure exerted on the slabs is not uniform because it depends on the relative location between the explosives and the slab, the shock wave motion direction and structural component distribution. The most common damage index for assessing the dynamic response of slabs is the plastic strain to show the cracking patterns comparing PE22 values with concrete cracking strain by 0.001333. Figure 11 shows the combined curve for maximum plastic strain values PE22 along Axis 1-1 (axial strain for slab) of first floor according to guidelines by SCI, UFC and GSA.

The effect of live load has been observed in the portion of slab from 17.75 m till the end of it with a clear divergence of curve by SCI guideline. However, the maximum PE22 values obtained by UFC and GSA are nearly identical. As a result, when the live load is increased by 100 % from UFC to SCI, the maximum value of plastic strain PE22 has decreased by 6.794 % at 25.25 m. With the continued increase of live load by 300 % from GSA to SCI, the maximum value of plastic strain has decreased by 5.286 % at 25.25 m and instantly, by 90.621 % to be less than cracking strain limit (0.001333) at 40.25 m. Therefore, each curve by UFC and GSA guidelines have provided the greatest values while curve by SCI guidelines was the least.

Another check was made to prove that failing of concrete at locations directly subjected to explosion from 17.75 m to 32.75 m (charge range) was due to tension failure with cracks before the compressive crushing by checking stresses along tenths of seconds till end of explosion. As a result, the maximum recorded value of stress is 23.1726 MPa which is less than the strength of concrete B40. Then, cracks by tension failure have taken place first.
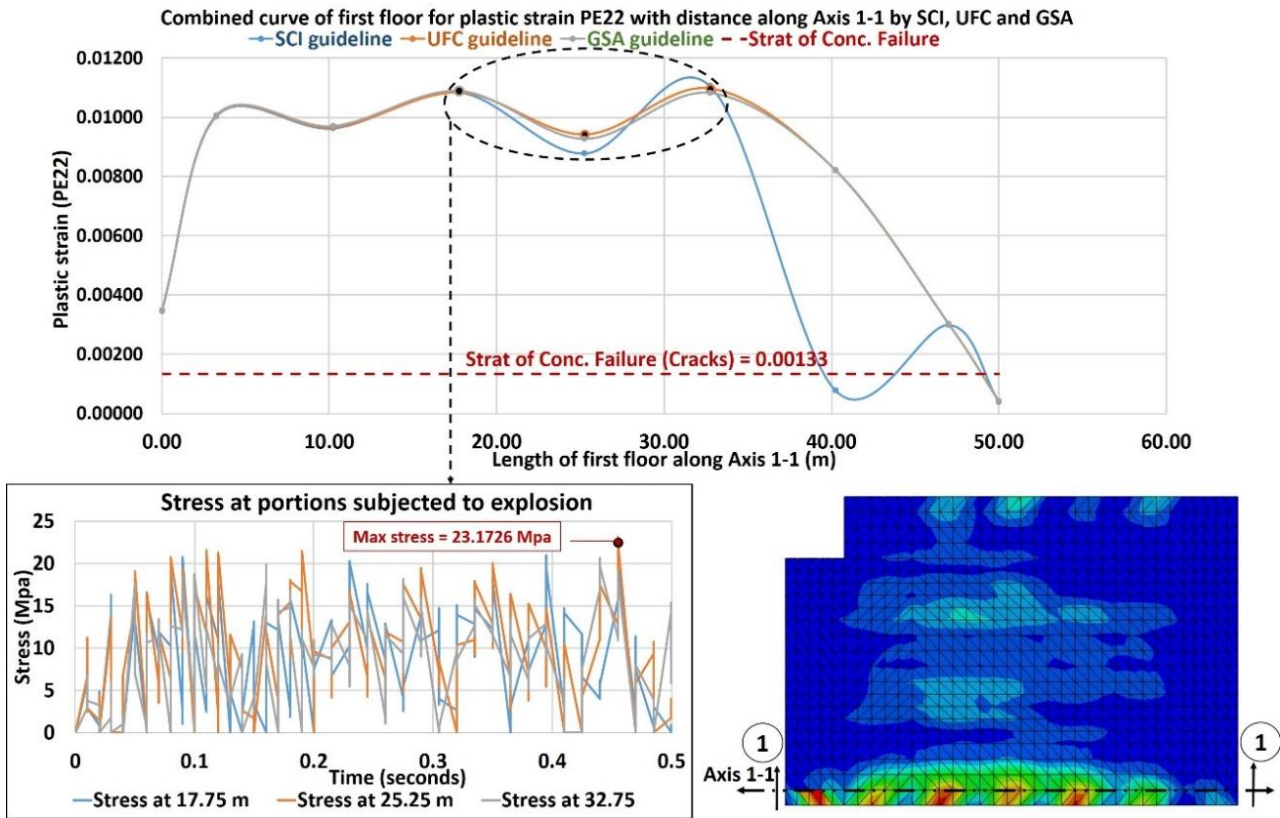
Figure 25: Combined curve for maximum values of plastic strain (PE22) along length of first floor according to guidelines by SCI, UFC and GSA

2.3.3. Damage assessment of main beams

As well for beams, the distribution of pressure is not uniform. The blast pressure wave begins to deviate from a totally plane shape as the scaled distance from explosive charge to beams decreases, affecting the blast pressure distribution on the target surface of beams. The most common damage index for assessing the dynamic response of beams is the displacement of a chosen critical main beam with the highest values to be discussed below.

Figure 12 illustrates vertical displacement contour for all beams at level 1 by GSA with an observed upper curvature at the portion in close proximity to the explosive charge that is directly hit more by the blast overpressure, especially at the shown main beam connecting between column C4 and C12.
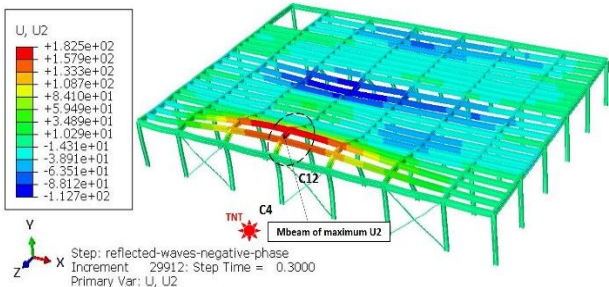
Then, the combined curve of maximum vertical displacement values for each guideline is shown in Figure 13. The effect of live load has been observed in range of mid span from 1.775 m to 5.325 m. As a result, when the live load is increased by 100 % from UFC to SCI, the value of maximum displacement has decreased by 1.872 % at mid span. With the continued increase of live load by 300 % from GSA to SCI, the value of maximum displacement has decreased by 3.311 % at mid span by 3.55 m, so that curve by GSA guideline has provided the greatest values while curve by SCI guidelines was the least.
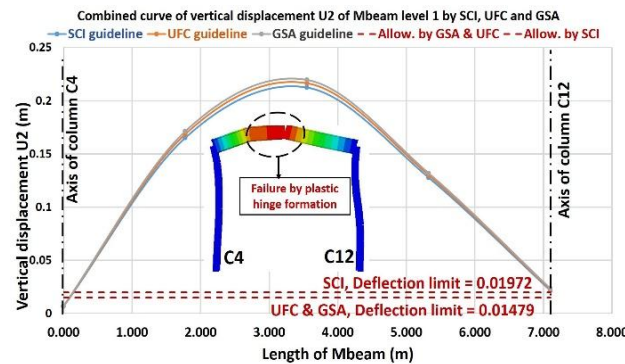

Figure 26: Vertical displacement (U2) for all beams at level 1 by GSA guideline

Figure 27: Combined deformed shape curve along length of main beam level 1 according to guidelines by SCI, UFC and GSA
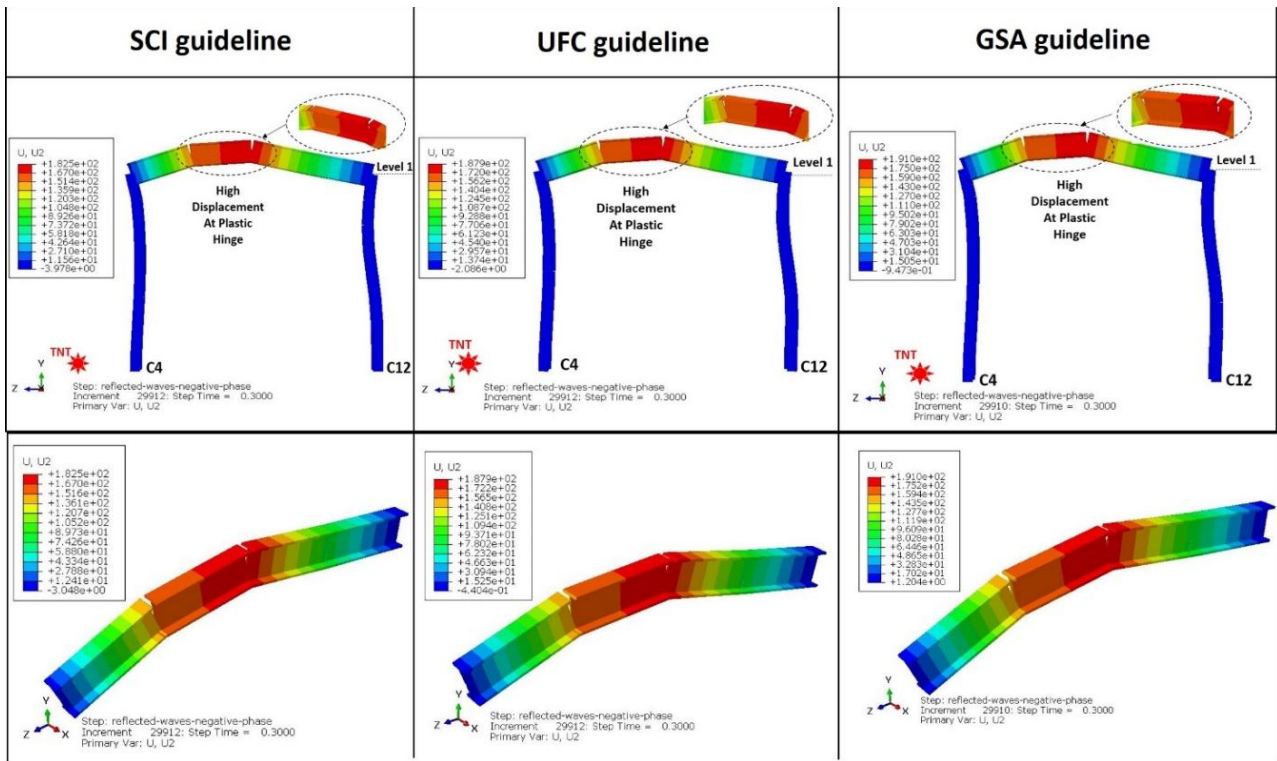
Figure 28: Upward deformation at mid-span of main beam level 1 according to guidelines by SCI, UFC and GSA

2.4 Damage Criteria

Evaluation of structure due to the extra-ordinary events like explosion is carried out by assessment of its damage by the criteria provided in the guidelines (SCI, UFC, and GSA) to check the durability and regularity whether for its elements or for its overall behavior and its material.

2.4.1. Deformation at plastic hinge of steel members

The nonlinear dynamic analysis performance evaluation criteria for steel members is based on displacement ductility and plastic hinge rotation [5, 7, 9, 10]. Plastic hinge rotation angle can be calculated based on the maximum displacement and member's length where the value of column's support rotation can be calculated by measuring the angle between vertical line and tangent to maximum deflected shape, which is determined by Equation 7 [42]:

$$\theta = tan^{-1}\left(\frac{\delta_{mid}}{0.5\,H}\right) \tag{7}$$

Where, θ, δ_{mid}, and H are the maximum support rotation, the midpoint displacement of column, and the column height, respectively. Among the general types of collapse mechanisms provided [43], the beam type is the critical collapse mechanism for this analysis due to the side effect of blast loading on the columns subjected to explosive charge. Since the plastic hinge formation is at the mid-height, top, or bottom region of these columns.

The other term is displacement ductility ratio (μ) which is defined as the ratio of maximum displacement of columns or beams at a reference point calculated using dynamic analysis to the elastic limit calculated using static linear analysis. Equation 8 defines it [5, 7, 9, 10, 44]:

$$\mu = \frac{\delta_{max}\,(dynamic\,analysis)}{\delta_e\,(static\,analysis)} \tag{8}$$

Where, δ_{max} and δ_e are the maximum displacement when the plastic hinge forms at a reference point and the elastic deflection limit, respectively. And they can be calculated directly from ABAQUS program.

Generally, increasing ductility is important such that the building parts can withstand deformations caused by the failure of a portion of the building's structure. For steel structures, increasing ductility is acquired by making connection stronger than the member itself or making columns stronger than beams so that columns resist loads better. In addition, increasing ductility in concrete constructions is accomplished by adding sufficient steel into concrete members.
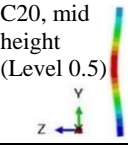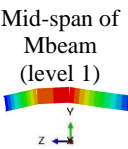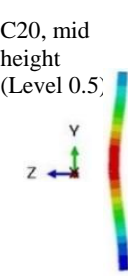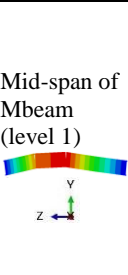
The nonlinear dynamic analysis performance evaluation criteria is based on the calculation of displacement ductility ratio and plastic hinge rotation, as shown in Table 9 for column C20 level 0.5 and mid span of main beam level 1. Criteria limits for the three guidelines are provided as:

- SCI allowable performance parameters for each material type and protection categories are defined

[7] for support rotation and ductility ratio limit. According to SCI guidelines, the given allowed ductility ratios are consistent with retaining structural integrity into the plastic range. As a result, the yielding portions associated with the hinge must be suitably constrained laterally to prevent premature failure due to instability and to justify the massive hinge rotations expected.

- UFC regulation is related to values of displacement ductility ratio that is produced in ASCE 41-13 [45]. On the other hand, values of plastic hinge rotation ratio limits is produced in the non-linear acceptance criteria of steel frames in the UFC 4-023-03 regulation [10], case of relatively flexure stiff connections.
- GSA regulation [9] provided values of rotation and ductility ratio to limit the possibility of collapse.

Table 9. Plastic hinge rotations and ductility ratios for column C20 level 0.5 and mid span on main beam level 1

Element	Guidelines	Displ. (mm)	Rotation Θ_{PH} °	Ductility μ
C20, mid height (Level 0.5)	SCI	367.882	6.991°	4.9004
	UFC	361.238	6.866 °	5.7263
	GSA	352.572	6.703 °	6.6750
Mid-span of Mbeam (level 1)	SCI	212.283	3.422 °	7.8713
	UFC	216.333	3.487 °	9.9294
	GSA	219.552	3.540 °	12.390

Element	Limit criteria Θ_{PH} °allow	Limit criteria μ allow	Comment "according to guidelines"
C20, mid height (Level 0.5)	12 ° Category (2)	20 Category (2)	Medium- High Damage, < limit
	2.005 ° Steel frames-flexure in tee	2 to 4 Non-linear procedure	High ductility demand, > limit
	1.861 ° St. columns	2.7144 St. columns	More than accepted limit
Mid-span of Mbeam (level 1)	12 ° Category (2)	20 Category (2)	Medium- High Damage, < limit
	2.005 ° Steel frames-flexure in tee	2 to 4 Non-linear procedure	High ductility demand, > limit
	1.861 ° St. columns	2.7144 St. columns	More than accepted limit

Both previous values of maximum ductility and maximum rotation for column C20 and main beam are within the SCI criteria. These elements are considered not susceptible to progressive collapse and its description comment is medium damage condition. On the other hand, values of maximum ductility and maximum rotation are out of the range of the UFC and GSA criteria for column C20 and main beam and their description comment is high ductility demand to collapse condition.

2.4.2. Criteria for DCRmoment/shear

Demand-Capacity-Ratio (DCR) is an indicative value used to assess the results of analysis and the magnitude as well as distribution of expected demands so that it is used only to determine structures' regularity. DCR for a given structural member can be determined as the ratio of the maximum demand (D) (e.g., moment, M_{max} or shear, Q_{max}) of the beam or column to its probable capacity (D) (e.g., ultimate moment capacity, M_p or ultimate shear capacity, Q_P).

$$DCR_{moment} = \frac{D}{C} = \frac{M_{max}}{M_P} \qquad (9)$$

$$DCR_{shear} = \frac{D}{C} = \frac{Q_{max}}{Q_P} \qquad (10)$$

Where, M_{max} is the calculated moment demand based on this dynamic analysis, and M_P is the moment capacity which is determined as the product of yield strength and plastic section modulus. Q_{max} is the shear force demand that is calculated from this dynamic analysis, and Q_P is the shear capacity which is the nominal shear strength of a web and is calculated by equation G2-1 of the ANSI-AISC 360-16 [35], knowing that for all ASTM W-shapes, σ_y is less than 345 Mpa.

Each of the regulations (SCI, UFC, and GSA) have produced their limits for DCR of moment or shear. UFC guideline is related to value of DCR by a value of 2 that is produced in ASCE 41-13 [45] at chapter 10, GSA guideline is related to value of DCR that is produced in section (4.1.2.3.1) by value of 2.0 for typical structural configurations with no transfer girders along one of the perimeter's faces. Section 4.1.2.3.2 by value of 1.5 for atypical structural configurations with transfer girders along one of the perimeter's faces for the evaluation of the potential for progressive collapse. In this study, there is no transfer girders so the DCR limit is 2 for typical structure and finally, SCI guideline has not provided any open data for demand-to-capacity so the limit can be taken by 2.0 as well.

In this research, the effect of the axial load was ignored when computing the M_p for columns for DCRmoment since it would reduce the value of pure plastic moment. Also all columns are I-sections with axial load less than 15% of the squash load (the product of yield stress and area section) before reaching the maximum plasticity. The pure plastic moment capacity is considered instead as the web carries the axial load while slightly contributing to the section's moment capacity.

DCRmoment for selected columns according to guidelines by SCI, UFC, and GSA guideline is shown in Figure 14. For any values of DCRmoment greater than 2.0,

the element is severely damaged as the component is expected to respond in moderate to high ductility demand so there is a high need for additional reinforcement or strengthening to meet the acceptance criteria.
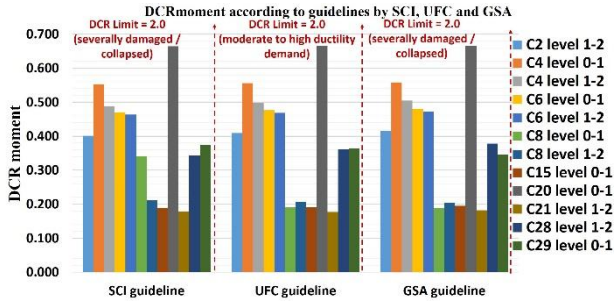
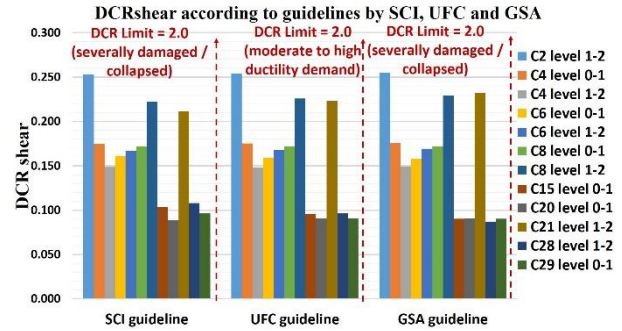**Figure 29: DCR for moment for selected columns according to guidelines by SCI, UFC, and GSA**

It can be noticed that columns C4 and C20 show the highest values of DCR_{moment}, among the other columns, indicating that they are the closest to start forming plastic hinges in which the section can rotate freely to undergo large strains during yielding to finally reduce the degree of redundancy. Theoretically, according to guidelines limits, as these DCR_{moment} values of all chosen columns are less than 2, the columns are adequate and does not need additional strengthening to meet the acceptance criteria and also have the potential to resist loads during time of explosion (0.5 seconds). However, once a column starts to form plastic hinge, it will collapse anyway over time by reaching the maximum plasticity after detonation and so that DCR is indicator for start of damage by plastic hinge.

In addition, the effect of increasing live load on DCR_{moment} values are almost similar between the three guidelines, except: when the live load is increased by 100 % from UFC to SCI for column (C8, level 0-1), the DCR_{moment} value has jumped immediately by 78.786 % and with the continued increase of live load by 300 % from GSA to SCI, the value has increased by 80.365 %.

For DCR_{shear}, the web will completely yield along before the flange begins to yield, so that yielding of the web represents one of the shear limit states. Mostly, DCR's for steel members is a function of section compactness and moment connection type.

Using the DCR criteria, columns with DCR_{shear} values greater than 2.0 is thought to be severely damaged or collapsed and has more damage potential which means that this member is expected to be a failed member. Therefore, sufficient strengthening is required to limit the DCR_{shear} values in accordance with the acceptance standards. In addition, it means the shear force demand has exceeded the shear capacity of section so the column connection to beams or foundation failed due to shear failure type (of bolts or plates) that occurs due to a lack of adequate shear resistance between the materials.

DCR_{shear} for selected columns according to guidelines by SCI, UFC and GSA guideline is shown in Figure 15. It is observed that DCR for shear force did not exceed the limit states.

Figure 30: DCR for shear for selected columns according to guidelines by SCI, UFC, and GSA

It can be noticed that in all scenarios studied, the DCR values of all chosen columns are less than 2, indicating that the columns are acceptable and have the potential to resist explosion. On the other hand, when identifying the effect of increasing of live load on DCR_{shear} values, the DCR_{shear} values are almost similar, except when the live load is increased by 100 % from UFC to SCI for column (C21, level 1-2), the value decreased by 5.118 %. And with the continued increase of live load by 300 % from GSA to SCI, the value increased by 8.698 %. In addition, when increasing live load by 100 % from UFC to SCI for column (C28, level 1-2), the value increased by 12.381 % and with the continued increase of live load by 300 % from GSA to SCI, the value jumped immediately by 23.911 %.

When comparing shear DCR values to bending DCR for the given columns in Figure 16 and Figure 17, the bending moment dominates more than the shear force for all columns, except column C21 level 1-2 and C8 level 1-2 in which shear force is the dominance to prove that DCR criterion should be shear-controlled when evaluating the likelihood of progressive collapse with blast loading as the initial cause of failure. Generally, because steel behaves equally in tension and compression, depending on the type of steel, it might be much weaker under shear loads, resulting in probable shear failure before attaining maximum compressive strength.
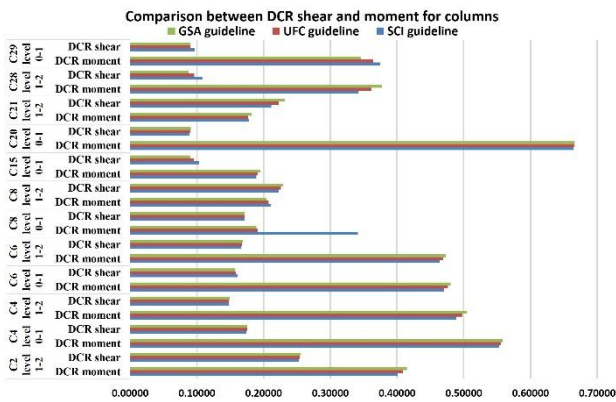
Figure 31: Comparison between DCR shear and moment for columns according to guidelines
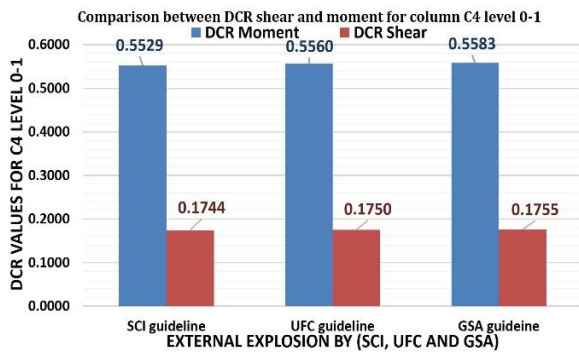

Figure 32: Dominance of the bending moment more than shear force of column C4

3. EVALUATION OF STABILITY AFTER EXPLOSION

As mentioned earlier, the failing members should be removed from the model, and all dead and live loads connected with them should be transferred to other members in neighboring bays. Then, the process of reloading with heat effect by the sudden loss of 15 columns that are expected to fail due to the initial formation of plastic hinges, has resulted in a stability in the model and it does not collapse, as shown in Figure 18 by UFC guideline (same stability for each model according to SCI and GSA guidelines).
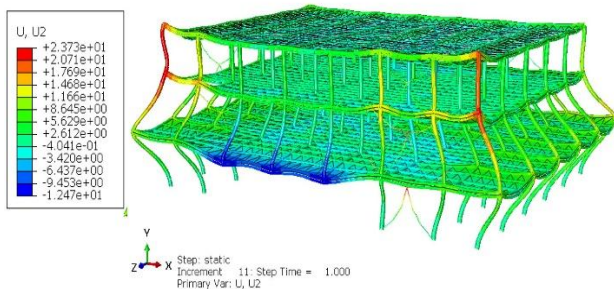

Figure 33: Overall displacement after explosion by ALP method using UFC guidelines

UFC guideline in process of reloading by ALP method is more realistic than the other guidelines as it provides two different load combinations one for bays close and the other for bays far from the removed columns that were subjected to explosive charge. Then, UFC guideline will be taken as a reference or indicator for predicting stability after explosion. It could be noticed that the frame at each section acts as one unit by its beams and columns at each level by a vierendeel effect and ductility of frame at connections which have prevented each frame from collapse despite columns loss, as shown in Figure 19 and Figure 20.
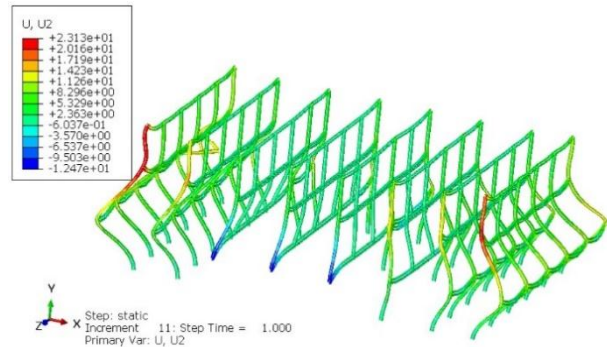

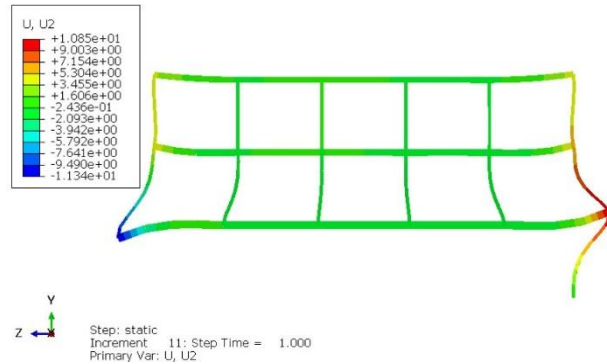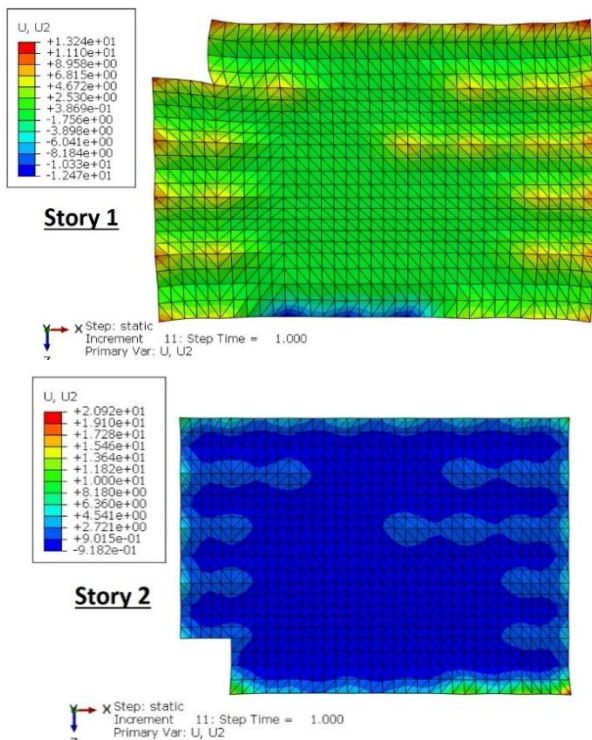**Figure 34: Geometry of main frames of the structure after removing columns**

Figure 35: Non-collapse of sectional frame by explosive charge by ALP method due to ductility and vierendeel effect

Also, the heat effect is noticed at the expansion of steel parts of beams and columns so that the first floor has expanded more than the second floor, as shown in Figure 21.

Figure 35: vertical displacement of concrete floors by ALP method, first floor (up) and second floor (down

Hence, according to the five general damage classes by [46], the damage level observed of the structure that is still partially usable is described by Class (D), due to damage at interior partitions and it can be repaired and reused again. Or by another classification of damage by [47], it is described as a moderate damage as the failure is within a localized area from the structure. In addition, Future work is needed for analysis model after explosion in detail.

4. CONCLUSIONS

A three-storey composite steel structure is subjected to 0.25 ton TNT by external explosion is studied dynamically taking into consideration the material nonlinearity at high strain rate according to criteria and load combinations of the common guidelines of explosions (SCI, UFC, and GSA). Direct simulation method is chosen for modelling blast loads on all members exposed to explosion. Evaluation of damage was introduced to assess the damage level of the members and the overall response of the proposed numerical model exposed to blast effects so that the following lines are some possible conclusions:

- One of the important blast effects not to be neglected on columns is the uplift of floors that causes the net upward loads at upper floors at external explosion.
- The influence of live load by load combination rules becomes more obvious when plastic strain

values are compared than internal force or displacement ones.

- Maximum absolute PE11 value of column C20 level 0-1 increased by 37.207 % at mid height when live load had increased by 300% from GSA to SCI. Hence, SCI guideline of total value of live load has provided the greatest absolute values of plastic strain while half percent of live load by UFC or quarter percent by GSA guidelines are the least.

- For slabs, when increasing live load by 100 % from UFC to SCI, the maximum value of plastic strain PE22 has decreased by 6.794 % at 25.25 m. With the continued increase of live load by 300 % from GSA to SCI, the maximum value of plastic strain PE22 has decreased by 5.286 % at 25.25 m and instantly, by 90.621 % to be less than limit of concrete failure at 40.25 m. Therefore, half percent of live load by UFC or quarter percent by GSA guidelines have provided the greatest values while total value of live load by SCI guideline was the least.

- There is no effect of reduction or increase of live load on equivalent plastic strain (PEEQ) at the plastic hinge position of column C20 after yielding as it is on the verge of failing due to increased loading by the time.

- Maximum displacement value at plastic hinge of column C20 increased with increasing live load by 1.839 % (UFC to SCI) and 4.342 % (GSA to SCI) within 0.365 seconds whereas maximum moment value decreased by 0.659 % (UFC to SCI) and 1.20 % (GSA to SCI) within 0.35 seconds at the same position. This prove that plastic hinge has no capability to resist moment or deformation by increasing time or live load.

- Column C4 that is subjected directly to explosive charge, has reached the maximum moment value within 0.15 seconds at level 1. Also, by increasing live load, its value decreased by 2.712 % (UFC to SCI) and 0.862 % (GSA to SCI) within the same time. Conversely, its maximum shear force is at level zero aligned to explosive charge within the same time by 0.15 seconds. Also, by increasing live load, its value decreased by 0.640 % (UFC to SCI) and 1.502 % (GSA to SCI) within the same time. All of these details illustrate how increasing live load at the same time reduces a section's capacity to endure internal forces (such as shear or moment).

- Due to uplift force from the explosion's entry at 0.05 seconds, Column C4 experienced its highest possible tensile stress of 210.729 Mpa. It is expected to fail by the time following the explosion (> 0.5 seconds) as the internal stress will exceed the tensile strength (270 Mpa).

- The majority of columns have surpassed the critical buckling load P_{cr} when checking the

failure due to buckling using Euler's buckling formula. Buckling then is prevalent, followed by a plastic hinge mechanism, an increase in global buckling and displacements, and finally column failure.

- According to guidelines limits, All of the columns' DCR_{moment} values are less than two, therefore they are all sufficient and don't need to be strengthened further to meet the acceptance criteria. However, DCR_{moment} values are indicator of which column, such as C4 or C20, the first possible plastic hinge could form.
- Bending moment is more effective when compared to shear force in DCR values for most selected columns. However, shear forces should be checked to avoid failure in connections or provide sufficient strengthening to limit the DCR_{shear} values according to approval requirements.
- The effects of increasing live load on $DCR_{shear/moment}$ values are nearly identical across the three standards.
- Beam evaluation criteria showed that it has medium to very high damage with high ductility demand at position of plastic hinge at mid-span.
- Stress is not enough for realizing failure of concrete parts as concrete is weak in tension and cracks would take place earlier at low stress values so that plastic strain is more effective.
- According to SCI guideline, it was found that it is overestimated the condition of an element forming plastic hinge.
- SCI guideline has un-provided data for DCR_{shear} or DCR_{moment} or for the load combination needed in case of removing damaged columns by ALP method after explosion.
- Values of plastic strains, displacement, rotation, and ductility ratio of SCI guideline are greater than those of UFC and GSA guidelines which were nearly close in most results.
- The static analysis at second stage of loading indicates that the frame is not likely to collapse by blast effects. In addition, Class D describes its damage level due to moderate damage.
- SCI guideline needs to include many limits for damage evaluation within and after explosions.

Further considerations
- More measurements for most elements need to be conducted in the future to choose the best overall guideline in each condition of evaluating damage.
- The study suggests considering the reflection phenomenon that raises the peak overpressure to a predetermined value known as reflected pressure by considering the incident pressure and reflected pressure coefficient.

5. REFERENCES

[1] P. A. Shirbhate, M.D.G., "A Critical Review of Blast Wave Parameters and Approaches for Blast Load Mitigation." Archives of computational methods in engineering, 2020.

[2] Ullah, A., et al., "Review of analytical and empirical estimations for incident blast pressure." 2017. 21(6): p. 2211-2225.

[3] Karlos, V. and G. Solomon, Calculation of blast loads for application to structural components, in Publications Office of the European Union. 2013. p. 1-58.

[4] Appuhamilage, G., Effects of Blast Loading on Reinforced Concrete Facade Systems. 2015, Victoria University.

[5] ENGINEERS, U.S.A.C.O., Unified Facilities Criteria (UFC) Structures To Resist the Effects of Accidental Explosions Approved for Public Release; Distribution Unlimited. 2005.

[6] Fu, F., "Advanced Modelling Techniques in Structural Design A Structural Equation Modeling Approach." First edition ed. 2015. 253.

[7] Yandzio, E. and M. Gough, Protection of buildings against explosions. 1999: Steel Construction Institute UK.

[8] Buwono, H. and S. Alisjahbana, "Modifications modeling friedlander s blast wave equation using 6 th order polynomial equations." 2020.

[9] GSA, U.J.W., DC, "Progressive collapse analysis and design guidelines for new federal office buildings and major modernization projects." 2003.

[10] DoD, U., Unified Facilites Criteria (UFC)–design of buildings to resist progressive collapse. 2016, UFC 4-023-03.

[11] Pordel Maragheh, B., A. Jalali, and S.M.J.I.J.o.E. Mirhoseini Hezaveh, "Effect of Initial Local Failure Type on Steel Braced Frame Buildings against Progressive Collapse." 2020. 33(1): p. 34-46.

[12] Ahmed Galal, M., M. Bandyopadhyay, and A.J.J.o.P.o.C.F. Krishna Banik, "Progressive Collapse Analysis of Three-Dimensional Steel–Concrete Composite Building due to Extreme Blast Load."2020. 34(3): p. 04020021.

[13] Wang, F., J. Yang, and Z.J.E.F.A. Pan, "Progressive collapse behaviour of steel framed substructures with various beam-column connections." 2020. 109: p. 104399.

[14] Papadrakakis, M., V. Papadopoulos, and V. Plevris, "Monte Carlo analysis for the blast resistance design and assessment of a reinforced concrete wall." 2013.

[15] Wang, X.-h., et al., "Blast-induced damage and evaluation method of concrete gravity dam subjected to near-field underwater explosion." 2020. 209: p. 109996.

[16] Larcher, M. and F.J.I.j.o.p.s. Casadei, "Explosions in Complex Geometries-A Comparison of Several Approaches. 2010." 1(2): p. 169-196.

[17] Jin, Z., et al., "Numerical study on the interaction between underwater explosion bubble and a moveable plate with basic characteristics of a sandwich structure." 2018. 164: p. 508-520.

[18] Draganić, H. and V.J.T.G. Sigmund, "Blast loading on structures." 2012. 19(3): p. 643-652.

[19] Talaat, M., et al., "Finite element analysis of RC buildings subjected to blast loading." 2022. 13(4): p. 101689.

[20] ARA. Products, S., Blast Design Software, Anti-Terrorist Blast (A.T.-BLAST); Version 3.0, Applied Research Associates, Inc.2022 :https://www.ara.com/at-blast/, Albuquerque, NM USA. 2000.

[21] Fu, F.J.J.o.C.s.r., "Dynamic response and robustness of tall buildings under blast loading." 2013. 80: p. 299-307.

[22] Bagheripourasil, M. and Y.J.J.o.R.i.C.E. Mohammadi, "Comparison between alternative load path method and a direct applying blast loading method in assessment of the progressive collapse." 2015. 3(2): p. 1-15.

[23] Pourasil, M.B., Y. Mohammadi, and A.J.K.J.o.C.E. Gholizad, "A proposed procedure for progressive collapse analysis of common steel building structures to blast loading." 2017. 21(6): p. 2186-2194.

[24] Larcher, M., F. Casadei, and G.J.P.O.o.t.E.U.d. Solomos, "Simulation of blast waves by using mapping technology in EUROPLEXUS." 2014. 10: p. 98310.

[25] Sideri, J., et al., "Distributed Column Damage Effect on Progressive Collapse Vulnerability in Steel Buildings Exposed to an External Blast Event." Journal of Performance of Constructed Facilities, 2017. 31(5): p. 04017077-04017077.

[26] Abdallah, M.J.I.J.o.C. and E. Engineering, "Numerical Study of Steel Structures Responses to External Explosions." 2020. 14(4): p. 117-125.

[27] Dinu, F., et al., "Full-scale two-story steel frame building under near-field explosions." 2019.

[28] CEN-EC, E.J.B.E.C.f.S., 1-7: Eurocode 1–actions on structures: general actions–accidental actions. 2006.

[29] Manual, A.U.s.J.I., Pawtucket, RI, Version 6.14-1 [Computer software], hibbitt, karlsson and sorensen. 2004.

[30] KUSUMANINGRUM, P., "Numerical Modeling of RC and ECC encased RC columns subjected to close-in explosion." 2010.

[31] Duc Ngo, T., "Blast loading and blast effects on structures-an overview." 2007.

[32] Astaneh-Asl, A.J.S.T.R., Notes on blast resistance of steel and composite building structures. 2010.

[33] Tolcha, M.A.J.I.J.o.E.R., "Modelling plastic deformation of A36 mild steel under extrusion process." 2014. 3(7).

[34] Hafezolghorani, M., et al., "Simplified damage plasticity model for concrete." 2017. 27(1): p. 68-78.

[35] Fisher, J.M. Specification for structural steel buildings. 2005. AISC.

[36] Wang, X. and J.J.I.J.o.I.E. Shi, "Validation of Johnson-Cook plasticity and damage model using impact experiment." 2013. 60: p. 67-75.

[37] W.K. Chow, W.Y.H., Review on the requirements on fire resisting construction. International Journal on Engineering Performance-Based Fire Codes, 2002. 4(3): p. 68-83.

[38] Szyniszewski, S.T., "Progressive collapse of moment resisting steel framed buildings quantitative analysis based energy approach." 2008: University of Florida.

[39] Al-Thairy, H.J.A.i.M.S. and Engineering, "Behaviour and failure of steel columns subjected to blast loads: Numerical study and analytical approach." 2018. 2018.

[40] Bangash, M.Y.H., Structural detailing in steel: a comparative study of British, European and American codes and practices. 2000: Thomas Telford.

[41] Wight, J. and B.J.A.C.I.P. Rabbat, USA, Building Code Requirements for Structural Concrete and Commentary (ACI 318M-05). 2005.

[42] Krauthammer, T., Modern protective structures. Vol. 22. 2008: Crc Press.

[43] Wong, M.B., "Plastic analysis and design of steel structures." 2011: Butterworth-Heinemann.

[44] Carter, A., Department of Defense Accomplishments (2009-2016): Taking the Long View, Investing for the Future. 2017.

[45] ASCE. Seismic evaluation and retrofit of existing buildings. 2014. American Society of Civil Engineers Reston, VA.

[46] Kinney, G.F. and K.J. Graham, Explosive shocks in air. 2013: Springer Science & Business Media.

[47] Hinman, E. and P.H.C.J.W.B.D.G. Engineers, Blast safety of the building envelope. 2011.